Received 24 July 2024; accepted 15 August 2024. Date of publication 20 August 2024; date of current version 27 August 2024.

Digital Object Identifier 10.1109/OJCOMS.2024.3445990

Unveiling New Frontiers of Downlink Training in User-Centric Cell-Free Massive MIMO

GUILLEM FEMENIAS (Senior Member, IEEE), AND FELIP RIERA-PALOU (Senior Member, IEEE)

Mobile Communications Group and Artificial Intelligence Research Institute, University of the Balearic Islands, 07122 Palma, Spain

CORRESPONDING AUTHOR: G. FEMENIAS (e-mail: guillem.femenias@uib.es)

This work was supported in part by IRENE-STARMAN, funded by MCIU/AEI/10.13039/501100011033, Spain, under Grant PID2020-115323RB-C32; in part by GERMINAL, funded by MCIU/AEI/10.13039/501100011033, Spain, under Grant TED2021-131624B-I00; and in part by the European Union "NextGenerationEU"/PRTR.

ABSTRACT Cell-free massive MIMO (CF-mMIMO) emerges as a pivotal technology in the landscape of beyond-5G and 6G wireless networks, addressing the ever-increasing demand for seamless connectivity and unprecedented data throughput. This paper undertakes a comprehensive exploration of scalable user-centric (UC) CF-mMIMO systems, focusing on critical aspects of downlink (DL) channel state information (CSI) acquisition and its intricate interactions with both distributed and centralized precoding strategies. The paper delves into the crucial role of DL CSI acquisition, particularly in scenarios of weak channel hardening arising from sparse subsets of access points (APs) serving specific mobile stations (MS) in UC strategies, and transmission over spatially correlated multiple keyhole Ricean fading channels. The main contributions of this research work include in-depth analyses of different detection schemes under varying precoding scenarios, offering valuable insights for practical deployment. The pivotal role of DL CSI acquisition in optimizing the performance of UC CF-mMIMO networks is fully assessed, dismissing the use of DL pilot-based detection approaches and advocating for either centralized precoding architectures with statistical CSI-based decoding strategies at the MSs or distributed precoding schemes with DL blind channel estimation-based decoders at the MSs.

INDEX TERMS Cell-free massive MIMO, user-centric, scalability, keyhole channels, downlink training, channel hardening.

I. INTRODUCTION

A. CONTEXT AND PREVIOUS ART WORK

EMERGING as one of the most promising wireless networking technologies, cell-free massive MIMO (CF-mMIMO) addresses the pervasive connectivity demands and escalating data traffic needs in the realms of beyond-fifth generation (5G) and sixth generation (6G) networks [1], [2]. In a CF-mMIMO network, a large number of access points (APs), spread across a wide coverage area and typically equipped with small antenna arrays, collaboratively serve multiple mobile stations (MSs). The collective number of antennas across all APs far exceeds the count of MSs scheduled concurrently within the same time-frequency resources. Consequently, CF-mMIMO systems can be considered as a synergistic combination of ultra-dense networks (UDNs), massive multiple-input multiple-output (MIMO), and network MIMO, leveraging the advantages of each of them to deliver ubiquitous connectivity with uniformly high spectral and energy efficiencies (see, for instance, [3] and references therein).

The acquisition of accurate channel state information (CSI) is crucial in CF-mMIMO networks, as it enables the precoders at the transmitter and the combiners at the receiver to effectively adapt to the short-term time-frequency variations in the propagation channels. In these scenarios, time division duplex (TDD) operation is preferred for CSI acquisition because it allows APs to obtain uplink (UL) CSI from UL pilot transmissions by the MSs and leverage UL-downlink (DL) channel reciprocity to use it also as a proper DL CSI. This approach ensures that the required pilot resources are

proportional to the number of MSs and independent of both the number of APs and the number of antennas per AP.

To perform coherent detection and decoding of DL data, MSs must use an estimate of the effective DL channel gain and the variance of the effective noise (i.e., interference plus thermal noise) in the detection/decoding algorithm. The effective DL channel gain is a scalar, representing the inner product of the precoding and the channel vectors, and it undergoes short-term variations due to channel fading. A common approach in the CF-mMIMO literature is to assume that channel hardening occurs due to the large number of antennas used [3], [4]. Channel hardening is observed when the random realizations of the effective channel are close to the mean value (i.e., the variance is small), resulting in a consistent effective scalar channel across coherence blocks. This allows the system to be operated as if APs and MSs were communicating over a deterministic channel characterized by the mean of the effective DL channel, a scalar based on long-term statistics that can be safely assumed to be known at the MSs [3], [4]. The number of APs and the number of antennas per AP required to achieve channel hardening, however, strongly depend on the propagation environment, the precoder design, the user-centric (UC) policy used to associate MSs and APs or even the DL power control strategy implemented at the APs. In particular, results presented by Chen and Björnson in [5], where stochastic geometry tools were used to model the deployment of APs across the coverage area and uncorrelated Rayleigh fading was assumed, show that whether or not the channel hardens as the number of APs increases depends strongly on the propagation pathloss model. These authors also show that in this particular scenario, and for a given total number of antennas, hardening can be improved by using multi-antenna APs rather than single-antenna APs. Willhammer et al. in [6] experimentally show that channel hardening occurs in massive MIMO scenarios. However, they also show that the uncorrelated Rayleigh channel models commonly assumed in theoretical studies tend to provide overoptimistic performance metrics and do not accurately model the channel hardening metrics observed in realistic massive MIMO deployments. This discrepancy arises because real environments do not provide as rich scattering as assumed in the uncorrelated Rayleigh model, and line-of-sight (LOS) propagation paths can also play an important role in this particular context. In this regard, Álvarez-Polegre et al. in [7] show that under a spatially correlated Ricean fading channel and considering different precoding and combining strategies, the dominant LOS component of the Ricean fading has a positive impact both on the hardening of the channels as well as on the DL achievable spectral efficiencies. Interestingly, they also show that spatial antenna correlation degrades the channel hardening and rate performance when using a simple distributed conjugate beamforming (CB) precoder but improves this performance metric when implementing a centralized zero-forcing (ZF) precoding strategy. The use of more sophisticated distributed precoding schemes to enhance the channel hardening behavior has also been explored by Interdonato et al. in [8], Femenias et al. in [9] or Sutton et al. in [10]. In particular, these authors show that appropriately designing short-term normalized CB precoders, the channel hardening can be boosted thus enabling the MSs to reliably decode data relying on long-term statistical CSI.

In realistic scalable UC CF-mMIMO systems, the set of APs serving a particular MS might be rather sparse, the antennas at the APs might be correlated, there might be some of the propagation links between a particular MS and its serving APs that are in LOS and, moreover, there might be MSs being subject to propagation through keyhole channels [11], [12], [13]. In this situation, and based on the conclusions drawn from the evaluation of the aforementioned research work, channel hardening might be compromised. Therefore, using decoding strategies based solely on the availability of statistical CSI might not be appropriate. Under these circumstances, particularly when using distributed precoding schemes, a more effective approach to acquiring accurate CSI involves the APs transmitting beamformed DL pilots to help the MSs estimate the instantaneous effective DL channel [8]. Transmitting precoded DL pilots improves the quality of the CSI available at the MSs. However, it also consumes time-frequency resources that could otherwise be used to transmit DL payload data. Therefore, there is a clear trade-off between the performance improvement expected from the availability of instantaneous CSI and the performance degradation associated with the DL pilot transmission overhead. In [8], Interdonato et al. demonstrate that allowing the MSs to estimate the effective channel using DL pilots can significantly improve achievable spectral efficiency, especially in scalable UC CF-mMIMO deployments. A limitation of this work, however, is that the conclusions are solely based on results obtained for uncorrelated Rayleigh channels and assuming the use of distributed CB-based precoders.

Another method for acquiring instantaneous CSI is the blind channel estimation strategy. In this approach, the effective DL channel gains are estimated using the received DL payload data signals. Such an estimation method was developed by Ngo and Larsson in [13] for single-cell massive MIMO and was later generalized to a multi-cell massive MIMO network by Pasangi et al. in [14], assuming uncorrelated Rayleigh fading channels and simple CB precoders. In [15], Ghazanfari et al. proposed model-based and data-driven approaches for DL multi-cell massive MIMO blind channel estimation that accommodate spatially correlated Rayleigh fading, arbitrary linear precoding schemes, and generic pilot assignment strategies among MSs. Finally, Souza et al. in [16], investigated the performance of the blind estimation approach in UC CF-mMIMO networks under spatially correlated channels and considering different distributed precoding schemes, namely, the CB and the local partial-MMSE (LP-MMSE). The blind channel estimation approach has proven its capability to yield better estimates compared to simply using the mean of the effective channel gains, especially in scenarios with poor channel hardening

TABLE 1. Research gap analysis of the main bibliographical references.

	DL	Blind estimation	Keyhole channel	Ricean fading	Spatial correlation	CF-mMIMO	User-centric	Advanced precoders
Chen *et al.* [5]						✓		
Willhammer *et al.* [6]					✓			
Álvarez *et al.* [7]				✓	✓	✓	✓	✓
Interdonato *et al.* [8]	✓					✓	✓	
Femenias *et al.* [9]				✓	✓	✓	✓	
Sutton *et al.* [10]	✓		✓					
Ngo *et al.* [13]	✓	✓	✓					✓
Pasangi *et al.* [14]	✓	✓						
Ghazanfari *et al.* [15]	✓	✓			✓			✓
Souza *et al.* [16]	✓	✓			✓	✓	✓	

conditions. Additionally, it can outperform the pilot-based DL channel estimation approach by eliminating the necessity for additional pilot overhead.

B. MOTIVATION AND CONTRIBUTIONS

Summarizing the contributions of the aforementioned research works and in order to highlight the research gaps that are still left and which are intended to be fully addressed in this research work, Table 1 presents the research gap analysis of the main bibliographical references on this topic. As it can be observed, there is some previous art work dealing with the issue of channel hardening only in the UL, some of the bibliographical references have not considered the use of DL blind estimators, only two references have addressed propagation through keyhole scenarios, and Rice fading and/or spatially correlated fading have only been adequately treated in a few bibliographical references. Additionally, not all of the aforementioned bibliographical references are dedicated to the study of CF-mMIMO networks and even fewer to the study of scalable UC CF-mMIMO networks. It is also worth noting that most of these research works focus on studying the impact of channel hardening in systems that use low-complexity distributed precoders and do not evaluate the impact that the use of advanced centralized precoders might have on system performance. Hence, building on the background knowledge provided by the aforementioned earlier work and aiming at filling the gaps they have left, especially in the context of UC CF-mMIMO networks, our main goal in this paper is to provide solid answers to the following open questions:

- Considering that the number of APs serving an MS may be relatively small when implementing a scalable UC strategy, can it be ensured that all MSs in the system will experience sufficient channel hardening when relying on statistical CSI?
- Given that distributed precoding schemes based on CB tend to provide weak channel hardening metrics, particularly in scenarios involving multi-keyhole and spatially correlated fading channels, can these limitations be mitigated through the deployment of more advanced distributed precoders or even sophisticated centralized precoding techniques?
- Blind channel estimation schemes have demonstrated their ability to improve the DL performance of cellular massive MIMO systems, especially in environments with poor channel hardening. Can these schemes also deliver substantial performance gains in UC CF-mMIMO network deployments? Furthermore, how well do they adapt to environments characterized by multi-keyhole spatially correlated fading channels? Lastly, do blind channel estimation schemes outperform the traditional DL training-based methods?
- In the context considered in this paper, is it preferable to deploy a UC CF-mMIMO network with a large number of APs equipped with few antennas or fewer APs equipped with a large number of antennas? Should the same deployment strategy be followed regardless of the precoding scheme used at the APs?

In an effort to answer these and many other questions, the main contributions of this manuscript can be summarized as follows:

- A multiple keyhole spatially correlated Ricean fading channel model is introduced to examine the impact of channel hardening on system performance across diverse propagation conditions. The proposed model is general enough to encompass arbitrary channel models, ranging from purely spatially uncorrelated Rayleigh fading to spatially correlated keyhole propagation environments.
- Pilot-based UL and DL linear minimum mean square error (MMSE) channel estimators have been designed to operate under the generalized multiple keyhole spatially correlated Ricean fading channel model proposed in this work. To properly assess the performance provided by the pilot-based DL linear MMSE channel estimator under various system configurations, different scalable linear precoders are considered including the distributed CB and LP-MMSE precoders [3], as well as the centralized improved partial MMSE (IP-MMSE) precoder [17].

Remarkably, analytical closed-form expressions for the DL linear MMSE channel estimator are computed when using CB-based precoding.

- Exploiting the asymptotic properties of the sample average power of the received signal samples per frame, a blind channel estimation scheme is also adapted to the generalized multiple keyhole spatially correlated fading channel model in UC CF-mMIMO environments, thus avoiding the use of DL training pilots. Again, all the terms in this estimator are computed in closed-form for the CB precoder.
- Achievable spectral efficiency expressions are derived for each of the DL decoding strategies under evaluation. These expressions are applicable regardless of the propagation conditions or the precoding strategy used at the APs. Closed-form expressions for the achievable spectral efficiencies are obtained when employing the distributed CB precoder. These expressions are then used to derive significant insights into the impact of system parameters on network performance.
- Extensive numerical results are provided, suggesting that performing channel estimation in the DL may be completely unnecessary when centralized precoding schemes are used, and that it can provide substantial improvements in system performance when implementing distributed precoders. Additionally, the results indicate that blind channel estimation schemes offer significantly superior performance compared to DL pilot-based channel estimation schemes.

C. PAPER ORGANIZATION AND NOTATIONAL REMARKS

The remainder of this paper is organized as follows. Section II describes the general system model including the proposed multiple keyhole spatially correlated Ricean fading channel characterizing the propagation between APs and MSs, the UL training phase, the DL payload data transmission phase and both the blind and pilot-based DL channel estimation processes. The hardening ratio and achievable spectral efficiency are fully evaluated in Section III. Numerical results and discussions are set forth in Section IV, while the conclusions are summarized in Section V. For convenience, the most important acronyms and related descriptions are reproduced in alphabetical order in Table 2.

Notation: Vectors and matrices are denoted by lower- and upper-case boldface symbols. The q-dimensional identity matrix is represented by $\boldsymbol{I}_q$. The operators $\boldsymbol{X}^{-1}$, $\boldsymbol{X}^T$, $\boldsymbol{X}^*$ and $\boldsymbol{X}^H$ denote the inverse, transpose, conjugate and conjugate transpose (also known as Hermitian) of matrix $\boldsymbol{X}$, respectively. The expectation operator is denoted by $\mathbb{E}\{\cdot\}$. Finally, $\mathcal{CN}(\boldsymbol{m}, \boldsymbol{R})$ denotes a circularly symmetric complex Gaussian vector distribution with mean $\boldsymbol{m}$ and covariance $\boldsymbol{R}$, and $\mathcal{N}(0, \sigma^2)$ denotes a real valued zero-mean Gaussian random variable with standard deviation σ.

TABLE 2. List of main acronyms (in alphabetical order).

Acronym	Description
5G	Fifth generation
6G	Sixth generation
AP	Access point
BBD	Blind-based detection
CB	Conjugate beamforming
CF-mMIMO	Cell-free massive MIMO
CPU	Central processing unit
CSI	Channel state information
DCC	Dynamic cooperation clustering
DL	Downlink
HBD	Hardening-based detection
IP-MMSE	Improved partial-MMSE
LP-MMSE	Local partial-MMSE
LOS	Line-of-sight
MIMO	Multiple-input multiple-output
MMSE	Minimum mean square error
MS	Mobile station
NLOS	Non-line-of-sight
PBD	Pilot-based detection
SINR	Signal-to-interference-plus-noise ratio
TDD	Time division duplex
UC	User-centric
UL	Uplink

II. SYSTEM MODEL

Let us consider a CF-mMIMO network where M APs, each equipped with an array of N antennas, simultaneously serve K single-antenna MSs in the same frequency band. The APs, indexed by the set $\mathcal{M} = \{1, \ldots, M\}$, are randomly distributed across a large geographical area, and are all connected via fronthaul links to a central processing unit (CPU) (or multiple interconnected CPUs). The MSs, indexed by the set $\mathcal{K} = \{1, \ldots, K\}$, are uniformly spread on the coverage area of the network. Assuming a scalable user-centric dynamic cooperation clustering (DCC) implementation of the CF-mMIMO network, a MS $k \in \mathcal{K}$ is served by a subset $\mathcal{M}_k = \{m_{k1}, \ldots, m_{kM_k}\} \subseteq \mathcal{M}$ of $M_k \leq M$ APs [3].

As usually done in the context of massive MIMO communications, a standard block-fading channel model is considered where the channel response is assumed to be constant in a time-frequency coherence block of size τ_c samples (or channel uses) and that varies independently between successive coherence blocks. The CF-mMIMO network operates using a TDD protocol, where the frames, with a size of τ_f samples, are assumed to fit within the channel coherence block (i.e., $\tau_f \leq \tau_c$). Depending on the DL transmission strategy under consideration, the TDD frame is organized as follows:

- *No DL Pilot Transmission:* In this case, the TDD frame includes three phases, namely, the UL training phase, the UL payload data transmission phase and the DL payload data transmission phase, of sizes τ_{p_u}, τ_u and

τ_d samples, respectively, with $\tau_f = \tau_{p_u} + \tau_u + \tau_d$. During the UL training phase, the MSs transmit their pilot sequences to the APs that estimate the propagation channels corresponding to the MSs they serve. At the MSs, two detection strategies can be implemented, namely, the hardening-based detection (HBD) and the blind channel estimation-based detection (BBD) schemes. The HBD strategy assumes that a sufficient degree of channel hardening holds for the CF-mMIMO scenario under consideration, allowing the MSs to reliably decode the DL payload data by relying exclusively on the knowledge of statistical CSI. The BBD strategy, in contrast, does not rely on channel hardening and, instead, the MSs implement an explicit estimate of their instantaneous effective DL channels. Since the APs do not transmit DL pilots, the MSs must necessarily implement a blind channel estimation process.

- *DL Pilot Transmission:* In this case, the TDD frame includes an additional DL training phase, of size τ_{p_d} samples, in between the UL and DL payload data transmission phases, with $\tau_f = \tau_{p_u}+\tau_u+\tau_{p_d}+\tau_d$. During the DL training phase, the APs transmit precoded pilot sequences to the MSs that, in this way, are able to obtain pilot-based instantaneous CSI that can be used to improve the quality of the detection process. In the sequel, this will be denoted as the pilot-based detection (PBD) strategy. It is important to note that, as the size of the frame is fixed, the more samples are dedicated to the transmission of DL pilots, the fewer samples can be dedicated to the other phases of the TDD frame. Thus, assuming that the introduction of the DL training phase should not affect the sizes of the UL training and payload data transmission phases, transmitting DL pilots will unavoidably decrease the number of samples that can be dedicated to the DL payload data transmission phase and thus compromise the achievable spectral efficiency metrics.

A. CHANNEL MODEL

The propagation channel between the kth MS and the mth AP is denoted by the N-dimensional complex-valued vector $\boldsymbol{h}_{mk} \in \mathbb{C}^{N\times 1}$. In order to examine the impact of channel hardening on system performance across diverse propagation conditions, a model called generalized multiple keyhole spatially correlated Ricean fading channel is proposed. A schematic representation of some examples of the generalized multiple keyhole channel model is presented in Fig. 1. Within the framework of this propagation model, the aforementioned channel vector can be characterized as

$$\boldsymbol{h}_{mk} = \sum_{j=1}^{N_{mk}} c_{mkj}\alpha_{mkj}\boldsymbol{g}_{mkj}, \tag{1}$$

where N_{mk} is the number of effective keyholes around MS k as observed by AP m, c_{mkj} is the deterministic complex gain

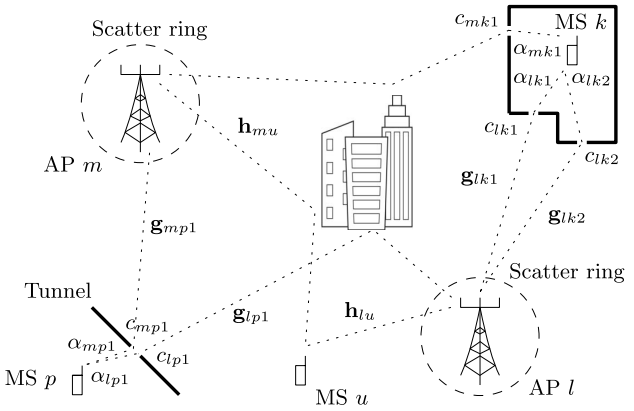

FIGURE 1. Schematic representation of some examples of the generalized multiple keyhole channel model: pure Ricean fading channel between MS u and AP l, pure Rayleigh fading channel between MS u and AP m, single keyhole Ricean fading channel between MS p and AP m, single-keyhole Rayleigh fading channels between MSs p and k and APs l and m, respectively, and finally, double-keyhole Ricean fading channel between MS k and AP l.

of the jth keyhole, which is assumed to be normalized such that $\sum_{j=1}^{N_{mk}} |c_{mkj}|^2 = 1$, α_{mkj} denotes the random channel gain between MS k and the jth keyhole, and $\boldsymbol{g}_{mkj}$ is the random channel vector between the jth keyhole and the mth AP. The channel gains between a MS and its associated keyholes are independent and distributed as $\alpha_{mkj} \sim \mathcal{CN}(0, 1)$. The channel vectors between a keyhole and the corresponding APs are modeled as spatially correlated Ricean fading channels with

$$\boldsymbol{g}_{mkj} = \sqrt{\frac{K_{mk}}{K_{mk}+1}}\chi_{mkj}\boldsymbol{a}(\varphi_{mk}, \vartheta_{mk}) + \sqrt{\frac{1}{K_{mk}+1}}\boldsymbol{q}_{mkj}, \tag{2}$$

where K_{mk} is the so-called Ricean K-factor, $\chi_{mkj} \sim \mathcal{CN}(0, \beta_{mk})$ is the random channel gain of the LOS component of the Ricean channel, with β_{mk} denoting the average channel propagation gain, $\boldsymbol{a}(\varphi_{mk}, \vartheta_{mk})$ is used to denote the array response vector at the azimuth and elevation angles φ_{mk} and ϑ_{mk} of the LOS propagation channel between the kth MS and the mth AP, with $\|\boldsymbol{a}(\varphi_{mk}, \vartheta_{mk})\|^2 = N$, and finally, the non-line-of-sight (NLOS) component is modeled as $\boldsymbol{q}_{mkj} \sim \mathcal{CN}(\boldsymbol{0}, \boldsymbol{C}_{mk})$, with $\boldsymbol{C}_{mk} \in \mathbb{C}^{N\times N}$ denoting the corresponding positive semi-definite spatial correlation matrix and holding $\mathrm{tr}(\boldsymbol{C}_{mk}) = N\beta_{mk}$.

The jth Ricean component of $\boldsymbol{h}_{mk}$ is distributed as $\boldsymbol{g}_{mkj} \sim \mathcal{CN}(\boldsymbol{0}, \boldsymbol{G}_{mk})$, with

$$\boldsymbol{G}_{mk} = \frac{K_{mk}}{K_{mk}+1}\beta_{mk}\boldsymbol{A}_{mk} + \frac{1}{K_{mk}+1}\boldsymbol{C}_{mk}, \tag{3}$$

where $\boldsymbol{A}_{mk} = \boldsymbol{a}(\varphi_{mk}, \vartheta_{mk})(\boldsymbol{a}(\varphi_{mk}, \vartheta_{mk}))^H$. The multiple keyhole spatially correlated Ricean fading channel, modeled as the sum of products of Gaussian random variables, is a zero-mean random vector whose positive semi-definite spatial correlation matrix can be obtained in closed form as

$$\begin{aligned}\boldsymbol{R}_{mk} &= \mathbb{E}\left\{\boldsymbol{h}_{mk}\boldsymbol{h}_{mk}^H\right\} \\ &= \sum_{j=1}^{N_{mk}}\sum_{j'=1}^{N_{mk}} c_{mkj}c_{mkj'}^* \mathbb{E}\left\{\alpha_{mkj}\alpha_{mkj'}^*\right\}\mathbb{E}\left\{\boldsymbol{g}_{mkj}\boldsymbol{g}_{mkj'}^H\right\} \\ &= \sum_{j=1}^{N_{mk}} \left|c_{mkj}\right|^2 \boldsymbol{G}_{mk} = \boldsymbol{G}_{mk}. \end{aligned} \tag{4}$$

B. UL TRAINING PHASE

During the UL training phase, MSs transmit pilot sequences of τ_{p_u} symbols to enable the APs performing channel estimation. Note that, in this case, the number of available orthogonal pilot sequences is equal to τ_{p_u}. The pilot sequence allocated to MS k is denoted by $\boldsymbol{\varphi}_{uk}$ and is drawn from a set of τ_{p_u} orthonormal sequences (i.e., $\|\boldsymbol{\varphi}_{uk}\|^2 = 1$ and $\boldsymbol{\varphi}_{u\,k}^H\boldsymbol{\varphi}_{ul} = 0$ for all $\boldsymbol{\varphi}_{ul} \neq \boldsymbol{\varphi}_{uk}$). The $N \times \tau_{p_u}$ received signal matrix at the mth AP during the UL training phase can be expressed as

$$\boldsymbol{Y}_m = \sum_{k\in\mathcal{K}} \sqrt{\tau_{p_u}P_{p_u}}\boldsymbol{h}_{mk}\boldsymbol{\varphi}_{u\,k}^T + \boldsymbol{N}_m, \tag{5}$$

where P_{p_u} is the transmit power per pilot symbol at the MSs, and $\boldsymbol{N}_m$ is an $N \times \tau_{p_u}$ matrix of independent and identically distributed (iid) additive noise samples with each entry distributed as $\mathcal{CN}(0, \sigma_u^2)$. If needed,[1] sufficient statistics to estimate $\boldsymbol{h}_{mk}$ can be obtained by projecting $\boldsymbol{Y}_m$ onto $\boldsymbol{\varphi}_{uk}^*$ as

$$\boldsymbol{y}_{mk} = \boldsymbol{Y}_m\boldsymbol{\varphi}_{uk}^* = \sqrt{\tau_{p_u}P_{p_u}}\sum_{l\in\mathcal{P}_{uk}}\boldsymbol{h}_{ml} + \boldsymbol{N}_m\boldsymbol{\varphi}_{uk}^*, \tag{6}$$

where $\mathcal{P}_{uk}$ is the set of MSs sharing the same UL pilot sequence that has been allocated to MS k, including itself. The linear MMSE estimate of $\boldsymbol{h}_{mk}$ can be obtained as [18]

$$\begin{aligned}\hat{\boldsymbol{h}}_{mk} &= \mathbb{E}\{\boldsymbol{h}_{mk}\boldsymbol{y}_{mk}^H\}\left(\mathbb{E}\{\boldsymbol{y}_{mk}\boldsymbol{y}_{mk}^H\}\right)^{-1}\boldsymbol{y}_{mk} \\ &= \sqrt{\tau_{p_u}P_{p_u}}\boldsymbol{R}_{mk}\boldsymbol{\Psi}_{mk}^{-1}\boldsymbol{y}_{mk}, \end{aligned} \tag{7}$$

where

$$\boldsymbol{\Psi}_{mk} = \mathbb{E}\{\boldsymbol{y}_{mk}\boldsymbol{y}_{mk}^H\} = \sum_{l\in\mathcal{P}_{uk}}\tau_{p_u}P_{p_u}\boldsymbol{R}_{ml} + \sigma_u^2\boldsymbol{I}_N. \tag{8}$$

Note that the linear MMSE channel estimates are zero-mean random vectors whose positive semi-definite spatial correlation matrices can be obtained as

$$\hat{\boldsymbol{R}}_{mk} = \tau_{p_u}P_{p_u}\boldsymbol{R}_{mk}\boldsymbol{\Psi}_{mk}^{-1}\boldsymbol{R}_{mk}. \tag{9}$$

Furthermore, even though the channel estimation vectors $\tilde{\boldsymbol{h}}_{mk} = \hat{\boldsymbol{h}}_{mk} - \hat{\boldsymbol{h}}_{mk}$ are not statistically independent of the corresponding linear MMSE channel estimates, they are uncorrelated and, hence, $\tilde{\boldsymbol{h}}_{mk}$ is a zero-mean random vector whose positive semi-definite spatial correlation matrix is

$$\tilde{\boldsymbol{R}}_{mk} = \boldsymbol{R}_{mk} - \hat{\boldsymbol{R}}_{mk}. \tag{10}$$

[1]Note that the mth AP will only estimate the channel of MS k if it participates in the combining and/or precoding of signals received from and/or transmitted to this particular MS.

Denoting by $\mathcal{D}_m$ the set of MSs served by the mth AP, and assuming that each of the MSs in $\mathcal{D}_m$ uses a different pilot sequence (this is a condition typically enforced by the DCC algorithm), the computational complexity for UL channel estimation at AP m is equal to $|\mathcal{D}_m|(N\tau_{p_u} + N^2)$ complex multiplications per coherence block [3, Sec. 4.2].

C. DL PAYLOAD DATA TRANSMISSION PHASE

Let $\boldsymbol{s}_k = [s_k(1)\ldots s_k(\tau_d)]^T$ be the vector of symbols intended for MS k in a generic TDD frame, where it is assumed that $\mathbb{E}\{\boldsymbol{s}_k\boldsymbol{s}_k{}^H\} = \boldsymbol{I}_{\tau_d}$, and that $\mathbb{E}\{\boldsymbol{s}_k\boldsymbol{s}_l^H\} = \boldsymbol{0}$, for all $l \neq k$. Using this definition, the signal vector transmitted by the mth AP in the tth symbol period of the DL payload data transmission phase, with $t \in \{1, \ldots, \tau_d\}$, can be expressed as

$$\boldsymbol{z}_m(t) = \sum_{l\in\mathcal{K}_m}\boldsymbol{w}_{ml}s_l(t), \tag{11}$$

with

$$\mathbb{E}\left\{\|\boldsymbol{z}_m(t)\|^2\right\} = \sum_{l\in\mathcal{K}_m}\mathbb{E}\left\{\|\boldsymbol{w}_{ml}\|^2\right\} \leq P_d, \tag{12}$$

where $\mathcal{K}_m$ denotes the set of MSs being served by the mth AP, and P_d is the DL transmit power available at the APs.

Let us define $\boldsymbol{h}_{\mathcal{M}_l k} = [\boldsymbol{h}_{m_{l1}k}^T\ldots\boldsymbol{h}_{m_{lM_l}k}^T]^T$ as the collective channel between MS k and the set of APs serving MS l, and $\boldsymbol{w}_l = [\boldsymbol{w}_{m_{l1}l}^T\ldots\boldsymbol{w}_{m_{lM_l}l}^T]^T$ as the NM_l-dimensional precoding vector used to transmit data to MS l. Using these definitions, the received DL signal at MS k in the tth symbol period can be expressed as

$$\begin{aligned} y_{dk}(t) &= \sum_{m\in\mathcal{M}}\boldsymbol{h}_{mk}^H\boldsymbol{z}_m(t) + n_{dk}(t) \\ &= \sum_{l\in\mathcal{K}}a_{kl}s_l(t) + n_{dk}(t), \end{aligned} \tag{13}$$

where

$$a_{kl} = \boldsymbol{h}_{\mathcal{M}_l k}^H\boldsymbol{w}_l \tag{14}$$

is the effective precoded channel between MS k and the set of APs serving MS l, and $n_{dk}(t) \sim \mathcal{CN}(0, \sigma_d^2)$.

Even though the proposed framework is general enough to encompass any DL precoding scheme, three scalable linear precoders will be considered in the following subsections: the distributed CB precoder (also known as the maximal ratio transmission (MRT) precoder) [4], the distributed LP-MMSE precoder [3], and the centralized IP-MMSE precoder [17]. The selection of these precoders is not arbitrary. The CB precoder aims to maximize the fraction of transmitted power effectively conveyed from a particular AP to the desired MS, but it ignores the interference that the AP might cause to other MSs in the network. Despite providing modest spectral efficiencies, this precoder has the advantage of reducing the fronthaul signaling load while also entailing much lower computational complexity. Moreover, most of the analytical expressions involved in both the channel estimation process and the determination of the achievable spectral efficiency

can be computed in closed form, providing valuable insight into the behavior of the system under different scenarios. The centralized IP-MMSE precoder strikes a proper balance between achieving a strong received signal and suppressing interference, aiming to maximize the signal-to-interference-plus-noise ratio (SINR) based on the channel estimates and statistics available at the set of APs jointly serving a particular MS. This scalable centralized precoder provides spectral efficiencies very close to those achievable using the optimal non-scalable MMSE precoder. However, unlike the CB precoder, it does not allow the computation of the achievable spectral efficiency in closed form and can only be analyzed using numerical results obtained through Monte Carlo methods. In contrast to the centralized IP-MMSE scheme, the LP-MMSE precoder implemented at a specific AP utilizes solely the channel estimates and statistics associated with the MSs served by that AP. As anticipated, this precoder presents a trade-off between performance metrics and computational complexities as those demonstrated by the CB and IP-MMSE precoders. As with the IP-MMSE, its performance assessment must rely on Monte Carlo simulations. Recognizing that the list of scalable precoding methods that could be evaluated in the proposed user-centric CF-mMIMO scenario is extensive, including options like the local-partial regularized zero forcing (LP-RZF) or the partial regularized zero-forcing (P-RZF) precoders [3], the selected precoders (i.e., CB, LP-MMSE, and IP-MMSE) were chosen because they represent a range of performance and complexity levels that sufficiently illustrate the key trade-offs that might be confronted in CF-mMIMO networks.

The number of complex multiplications per coherence block required to compute the precoding vector used to convey payload data to a particular MS, including the computation of the channel estimates, is summarized in [3, Table 5.1]. Note that the computational complexity associated with the IP-MMSE precoder is the same as that associated with the P-MMSE precoder.

1) CENTRALIZED IP-MMSE PRECODING

In centralized DL operation, the precoding vector computed at the CPU to transmit DL payload data to MS k capitalizes on the UL-DL duality theorem [3] and can be expressed as

$$\boldsymbol{w}_k = \sqrt{p_{dk}} \frac{\overline{\boldsymbol{w}}_k}{\sqrt{\mathbb{E}\{\|\overline{\boldsymbol{w}}_k\|^2\}}}, \tag{15}$$

where p_{dk} is the transmit power allocated to MS k, and $\overline{\boldsymbol{w}}_k$ is the combining vector applied to MS k in the UL payload data transmission phase.

Relying on the large-scale CSI available at the CPU, the IP-MMSE combiner can be designed as [17]

$$\overline{\boldsymbol{w}}_k = \sqrt{p_{uk}} \boldsymbol{\Omega}_k^{-1} \hat{\boldsymbol{h}}_{\mathcal{M}_k k}, \tag{16}$$

where $p_{uk} \leq P_u$ is the UL transmit power allocated to MS k, with P_u denoting the transmit power available at the MSs, and

$$\boldsymbol{\Omega}_k = \sum_{l \in \mathcal{S}_k} p_{ul} \left(\hat{\boldsymbol{h}}_{\mathcal{M}_k l} \hat{\boldsymbol{h}}_{\mathcal{M}_k l}^H + \tilde{\boldsymbol{R}}_{\mathcal{M}_k l} \right) + \sum_{l \notin \mathcal{S}_k} p_{ul} \boldsymbol{R}_{\mathcal{M}_k l} + \sigma_u^2 \boldsymbol{I}_{M_k N}, \tag{17}$$

with $\mathcal{S}_k$ denoting the set of MSs that are served by partially the same network nodes as MS k, that is, $\mathcal{S}_k = \{l : \mathcal{M}_k \cap \mathcal{M}_l \neq \emptyset\}$, $\hat{\boldsymbol{h}}_{\mathcal{M}_k l} = [\hat{\boldsymbol{h}}_{m_{k1} l}^T \ldots \hat{\boldsymbol{h}}_{m_{kM_k} l}^T]^T$ denoting the MMSE estimate of the channel between MS l and the set of APs serving MS k, $\boldsymbol{R}_{\mathcal{M}_k l} = \text{blockdiag}(\boldsymbol{R}_{m_{k1} l}, \ldots, \boldsymbol{R}_{m_{kM_k} l})$, and $\tilde{\boldsymbol{R}}_{\mathcal{M}_k l} = \text{blockdiag}(\tilde{\boldsymbol{R}}_{m_{k1} l}, \ldots, \tilde{\boldsymbol{R}}_{m_{kM_k} l})$.

Inspired by the approach proposed by Nikbakht et al. in [19] and Chen et al. in [20], a scalable distributed UL fractional power control strategy was described by Demir et al. in [3, Sec. 7.2.1], where

$$p_{uk} = P_u \frac{\left(\sum_{m \in \mathcal{M}_k} \beta_{mk} \right)^{\upsilon}}{\max_{l \in \mathcal{S}_k} \left(\sum_{m \in \mathcal{M}_l} \beta_{ml} \right)^{\upsilon}}, \tag{18}$$

with the exponent $\upsilon \in [-1, 1]$ operating as a knob to modify the power control behavior, from a max-min fairness power allocation strategy to a sum-rate maximization approach.

In the DL, the power p_{dk} allocated to the kth MS is distributed among the channels of the different APs according to the normalized precoding vector described in (15). Although other scalable power allocation strategies can be found in the literature on CF-mMIMO (see, for example, [21], [22]), one of the proposals that has gained more acceptance in this research area is the one proposed by Demir et al. in [3, Sec. 7.2.2], where

$$p_{dk} = \frac{P_d \left(\sum_{m \in \mathcal{M}_k} \beta_{mk} \right)^{\upsilon} \omega_k^{-\kappa}}{\max_{m' \in \mathcal{M}_k} \sum_{l \in \mathcal{K}_{m'}} \left(\sum_{m \in \mathcal{M}_l} \beta_{ml} \right)^{\upsilon} \omega_l^{1-\kappa}}. \tag{19}$$

This proposal was inspired by the heuristic UL fractional power control strategy in (18) and incorporates, on the one hand, the power constraints at the APs and, on the other hand, the scaling parameters defined as

$$\omega_k = \max_{m \in \mathcal{M}_k} \frac{\mathbb{E}\{\|\overline{\boldsymbol{w}}_{mk}\|^2\}}{\mathbb{E}\{\|\overline{\boldsymbol{w}}_k\|^2\}}, \tag{20}$$

which prevent the transmit powers from being allocated in an overly conservative manner. The exponent $0 \leq \kappa \leq 1$ reshapes the ratio of power allocation between different MSs.

2) LOCAL TRANSMIT PRECODING

Assuming a distributed DL operation, a local transmit precoder can be implemented at each of the APs in the network. Assuming that AP m serves MS k (i.e., $k \in \mathcal{K}_m$), the corresponding precoding vector can be generically expressed as

$$\boldsymbol{w}_{mk} = \sqrt{p_{dmk}} \frac{\overline{\boldsymbol{w}}_{mk}}{\sqrt{\mathbb{E}\{\|\overline{\boldsymbol{w}}_{mk}\|^2\}}}, \tag{21}$$

where p_{dmk} denotes the DL transmit power allocated by the mth AP to MS k, and $\overline{\boldsymbol{w}}_{mk}$ is a vector pointing out the direction of the precoder. As suggested by Demir et al. in [3], two scalable versions of the local transmit precoder are worth considering. The first one, defined by

$$\overline{\boldsymbol{w}}_{mk} = \boldsymbol{\Lambda}_m^{-1}\hat{\boldsymbol{h}}_{mk}, \tag{22}$$

with

$$\boldsymbol{\Lambda}_m = \sum_{l\in\mathcal{K}_m} p_{ul}\left(\hat{\boldsymbol{h}}_{ml}\hat{\boldsymbol{h}}_{ml}^H + \tilde{\boldsymbol{R}}_{ml}\right) + \sigma_u^2\boldsymbol{I}_N, \tag{23}$$

is called the LP-MMSE precoder. The second one, known as the CB precoder, is defined by

$$\overline{\boldsymbol{w}}_{mk} = \hat{\boldsymbol{h}}_{mk}, \tag{24}$$

thus holding that $\mathbb{E}\{\|\overline{\boldsymbol{w}}_{mk}\|^2\} = \mathrm{tr}(\hat{\boldsymbol{R}}_{mk})$. Again, a fractional DL power allocation is considered for the distributed operation [3], [8], [19], where

$$p_{dmk} = \begin{cases} P_d \frac{\beta_{mk}^{\varpi}}{\sum_{l\in\mathcal{K}_m}\beta_{ml}^{\varpi}} & \text{if } k\in\mathcal{K}_m \\ 0, & \text{otherwise,} \end{cases} \tag{25}$$

with the exponent $\varpi \in [-1, 1]$ dictating the power control behavior, similar to υ in the centralized scenario.

D. DL BLIND CHANNEL ESTIMATION

Following the steps of the DL blind channel estimation technique proposed by Ngo and Larsson in [13] for a cellular massive MIMO scenario, when implementing the BBD strategy, the sample average power of the received signal $y_{dk}(t)$ during the DL payload data transmission phase of a generic TDD frame can be computed as

$$\xi_k = \frac{1}{\tau_d}\sum_{t=1}^{\tau_d}|y_{dk}(t)|^2. \tag{26}$$

When τ_d is large, the application of the law of large numbers allows the sample average ξ_k to be approximated as[2]

$$\xi_k \approx |a_{kk}|^2 + \varrho_k + \sigma_d^2, \tag{27}$$

with

$$\varrho_k = \sum_{\substack{l\in\mathcal{K}\\ l\neq k}}\mathbb{E}\left\{|a_{kl}|^2\right\}. \tag{28}$$

The variables ϱ_k, for all $k \in \mathcal{K}$, solely depend on large-scale CSI that remains almost invariant over many coherence blocks and can be straightforwardly computed at the MSs [4]. Therefore, taking into account that, with high probability, the real part of a_{kk} is much larger than the corresponding imaginary part (i.e., the phase of a_{kk} is approximately equal to zero) when M_kN is large, an estimate of a_{kk} can be obtained as [15]

$$\hat{a}_{kk}^{\mathrm{bbd}} = \begin{cases} \sqrt{\xi_k - \varrho_k - \sigma_d^2}, & \text{if } \xi_k > \theta_k \\ \mathbb{E}\{a_{kk}\}, & \text{otherwise,} \end{cases} \tag{29}$$

where $\hat{a}_{kk}^{\mathrm{bbd}}$ has been set equal to $\mathbb{E}\{a_{kk}\}$ when the argument of the square root is larger than θ_k. To ensure that the square root in (29) provides a real number, the value of the switching point θ_k between the two cases must hold that $\theta_k \geq \varrho_k + \sigma_d^2$.

Note that the estimate $\hat{a}_{kk}^{\mathrm{bbd}}$ obtained in (29) is correlated with all the symbols in $\boldsymbol{s}_k$ and, as shown in [13, Sec. V], this complicates the computation of an achievable spectral efficiency for this particular detection strategy. To address this issue, when computing the achievable spectral efficiency provided by the BBD scheme (see Section II-B2), the channel estimate that will be assumed to be used when detecting the tth DL payload data symbol at MS k will be obtained as

$$\hat{a}_{kk}^{\mathrm{bbd}} \approx \hat{a}_{kk}^{\mathrm{bbd}}(t) = \begin{cases} \sqrt{\xi_k(t) - \varrho_k - \sigma_d}, & \text{if } \xi_k(t) > \theta_k \\ \mathbb{E}\{a_{kk}\}, & \text{otherwise,} \end{cases} \tag{30}$$

where

$$\xi_k(t) = \frac{1}{\tau_d}\sum_{\substack{t'=1\\ t'\neq t}}^{\tau_d}|y_{dk}(t')|^2. \tag{31}$$

This guarantees that $\hat{a}_{kk}^{\mathrm{bbd}} \approx \hat{a}_{kk}^{\mathrm{bbd}}(t)$ is uncorrelated with $s_k(t)$.

Note that the computational complexity associated with the blind-based channel estimation (measured in terms of complex multiplications) may be considered negligible, as it only increases linearly with τ_d.

Theorem 1: For the distributed CB case, the APs (or the CPU) can compute the variables $\mathbb{E}\{a_{kk}\}$ and ϱ_k in closed form as

$$\mathbb{E}\{a_{kk}\} = \sum_{m\in\mathcal{M}_k}\sqrt{p_{dmk}\,\mathrm{tr}\left(\hat{\boldsymbol{R}}_{mk}\right)}, \tag{32}$$

and

$$\begin{aligned}\varrho_k = &\sum_{\substack{l\in\mathcal{K}\\ l\neq k}}\sum_{m\in\mathcal{M}_l}\frac{p_{dml}}{\mathrm{tr}\left(\hat{\boldsymbol{R}}_{ml}\right)}\mathrm{tr}\left(\boldsymbol{R}_{mk}\hat{\boldsymbol{R}}_{ml}\right)\\ &+\sum_{\substack{l\in\mathcal{P}_{uk}\\ l\neq k}}\left|\sum_{m\in\mathcal{M}_l}\sqrt{\frac{p_{dml}}{\mathrm{tr}\left(\hat{\boldsymbol{R}}_{ml}\right)}}\mathrm{tr}\left(\hat{\boldsymbol{R}}_{mk}\boldsymbol{R}_{ml}\boldsymbol{R}_{mk}^{-1}\right)\right|^2\\ &+\sum_{\substack{l\in\mathcal{P}_{uk}\\ l\neq k}}\sum_{m\in\mathcal{M}_l}\frac{p_{dml}}{\mathrm{tr}\left(\hat{\boldsymbol{R}}_{ml}\right)}\lambda_{mk}\\ &\times\left[\mathrm{tr}\left(\boldsymbol{R}_{mk}\boldsymbol{R}_{ml}\left(\boldsymbol{R}_{mk}^{-1}\hat{\boldsymbol{R}}_{mk}\right)^2\boldsymbol{R}_{mk}^{-1}\boldsymbol{R}_{ml}\right)\right.\\ &\left.+\mathrm{tr}\left(\hat{\boldsymbol{R}}_{mk}\boldsymbol{R}_{ml}\boldsymbol{R}_{mk}^{-1}\right)\mathrm{tr}\left(\hat{\boldsymbol{R}}_{mk}\boldsymbol{R}_{mk}^{-1}\boldsymbol{R}_{ml}\right)\right],\end{aligned} \tag{33}$$

[2]It is worth noting that, with high probability $|a_{kl}|^2 \ll |a_{kk}|^2$, for all $l \neq k$ and, hence, the approximation is still valid even for small values of τ_d.

respectively, where

$$\lambda_{mk} = \sum_{j=1}^{N_{mk}} \left| c_{mkj} \right|^4. \tag{34}$$

Proof: See Appendix B. ■

E. DL TRAINING PHASE IN THE PBD CASE

When implementing the PBD strategy, DL pilot sequences of τ_{p_d} symbols are beamformed to the MSs by using the same precoding filters that will be employed during the DL payload data transmission phase. Let us denote the DL pilot sequence allocated to MS k by $\boldsymbol{\varphi}_{dk}$. As in the UL, these pilot sequences are assumed to be drawn from a set of τ_{p_d} orthonormal sequences (i.e., $\|\boldsymbol{\varphi}_{dk}\|^2 = 1$ and $\boldsymbol{\varphi}_{dk}\boldsymbol{\varphi}_{dl} = 0$ for all $\boldsymbol{\varphi}_{dl} \neq \boldsymbol{\varphi}_{dk}$). Under these assumptions, the $N \times \tau_{p_d}$ signal matrix transmitted by the mth AP during the DL training phase can be expressed as

$$\boldsymbol{X}_m = \sqrt{\tau_{p_d}} \sum_{l \in \mathcal{K}_m} \boldsymbol{w}_{ml} \boldsymbol{\varphi}_{dl}^T. \tag{35}$$

Equivalently, the $N\tau_{p_d}$-dimensional vector of samples transmitted by the mth AP during the DL training phase can be written as

$$\begin{aligned} \boldsymbol{x}_m = \mathrm{vec}(\boldsymbol{X}_m) &= \sqrt{\tau_{p_d}} \sum_{l \in \mathcal{K}_m} \mathrm{vec}\left(\boldsymbol{w}_{ml} \boldsymbol{\varphi}_{dl}^T \right) \\ &= \sqrt{\tau_{p_d}} \sum_{l \in \mathcal{K}_m} \left(\boldsymbol{\varphi}_{dl} \otimes \boldsymbol{I}_N \right) \boldsymbol{w}_{ml}, \end{aligned} \tag{36}$$

and the average power spent by the mth AP to transmit the DL pilots can be obtained as

$$\begin{aligned} &\mathbb{E}\left\{ \|\boldsymbol{x}_m\|^2 \right\} \\ &\quad = \tau_{p_d} \sum_{l \in \mathcal{K}_m} \sum_{l' \in \mathcal{K}_m} \mathbb{E}\left\{ \boldsymbol{w}_{ml}^H \left(\boldsymbol{\varphi}_{d\,l}^H \boldsymbol{\varphi}_{dl'} \otimes \boldsymbol{I}_N \right) \boldsymbol{w}_{ml'} \right\}. \end{aligned} \tag{37}$$

The average transmit power must be constrained to ensure that $\mathbb{E}\{\|\boldsymbol{x}_m\|^2\} \leq \tau_{p_d} P_d$, and achieving this is quite difficult in a general setting where UL and/or DL pilot sequences are allocated arbitrarily. To address this issue, the DL pilot assignment is constrained such that, for any pair of MSs l and l' in $\mathcal{K}_m$, with $l \neq l'$, it holds $\boldsymbol{\varphi}_{d\,l}^H \boldsymbol{\varphi}_{dl'} = 0$. Note that this is tantamount to assume that a given AP can only serve up to τ_{p_d} MSs, and all of them are allocated orthogonal pilot sequences. Interestingly, this constraint is already imposed by the *classical* UL pilot allocation and DCC strategy proposed by Demir et al. in, and it can be readily extended to the DL scenario, as will be shown in the following subsections.[3] In this particular case, (37) simplifies to

$$\mathbb{E}\left\{ \|\boldsymbol{x}_m\|^2 \right\} = \tau_{p_d} \sum_{l \in \mathcal{K}_m} \mathbb{E}\left\{ \|\boldsymbol{w}_{ml}\|^2 \right\}, \tag{38}$$

which is equivalent to constraint (12).

The τ_{p_d}-dimensional row vector received at the kth MS during the DL training phase is given by

$$\boldsymbol{y}_{p\,k}^T = \sum_{m \in \mathcal{M}} \boldsymbol{h}_{mk}^H \boldsymbol{X}_m + \boldsymbol{n}_{p\,k}^T, \tag{39}$$

where $\boldsymbol{n}_{pk} \sim \mathcal{CN}(\boldsymbol{0}, \sigma_d^2 \boldsymbol{I}_{\tau_{p_d}})$. Sufficient statistics to estimate the effective precoded DL channel a_{kk} can be obtained by projecting the received signal vector onto the pilot sequence $\boldsymbol{\varphi}_{dk}{}^*$ as follows

$$\begin{aligned} \check{y}_{pk} = \boldsymbol{y}_{p\,k}^T \boldsymbol{\varphi}_{dk}{}^* &= \sum_{m \in \mathcal{M}} \boldsymbol{h}_{mk}^H \boldsymbol{X}_m \boldsymbol{\varphi}_{dk}{}^* + \check{n}_{pk} \\ &= \sqrt{\tau_{p_d}} \sum_{m \in \mathcal{M}} \boldsymbol{h}_{mk}^H \sum_{l \in \mathcal{K}_m} \boldsymbol{w}_{ml} \boldsymbol{\varphi}_{dl}{}^T \boldsymbol{\varphi}_{dk}{}^* + \check{n}_{pk} \\ &= \sqrt{\tau_{p_d}} \sum_{l \in \mathcal{P}_{dk}} a_{kl} + \check{n}_{pk}, \end{aligned} \tag{40}$$

where $\mathcal{P}_{dk}$ is the set of MSs sharing the same DL pilot sequence as MS k, including itself, and $\check{n}_{pk} = \boldsymbol{n}_{p\,k}^T \boldsymbol{\varphi}_{dk}{}^*$.

Given $\check{y}_{pk}$, the linear MMSE estimate of the effective precoded channel between MS k and the set of APs in $\mathcal{M}_k$ can be obtained as

$$\hat{a}_{kk}^{\mathrm{pbd}} = \mathbb{E}\{a_{kk}\} + \frac{\mathrm{cov}\{a_{kk}, \check{y}_{pk}\}}{\mathrm{var}\{\check{y}_{pk}\}} \left(\check{y}_{pk} - \mathbb{E}\{\check{y}_{pk}\} \right), \tag{41}$$

where

$$\mathbb{E}\{\check{y}_{pk}\} = \sqrt{\tau_{p_d}} \sum_{l \in \mathcal{P}_{dk}} \mathbb{E}\{a_{kl}\}, \tag{42a}$$

$$\mathrm{cov}\{a_{kk}, \check{y}_{pk}\} = \mathbb{E}\left\{ a_{kk} \check{y}_{pk}^* \right\} - \mathbb{E}\{a_{kk}\} \mathbb{E}\left\{ \check{y}_{pk}^* \right\}, \tag{42b}$$

$$\mathbb{E}\left\{ a_{kk} \check{y}_{pk}^* \right\} = \sqrt{\tau_{p_d}} \sum_{l \in \mathcal{P}_{dk}} \mathbb{E}\left\{ a_{kk} a_{kl}^* \right\}, \tag{42c}$$

$$\mathrm{var}\{\check{y}_{pk}\} = \mathbb{E}\left\{ \left| \check{y}_{pk} \right|^2 \right\} - \left| \mathbb{E}\{\check{y}_{pk}\} \right|^2, \tag{42d}$$

and

$$\mathbb{E}\left\{ \left| \check{y}_{pk} \right|^2 \right\} = \tau_{p_d} \sum_{l \in \mathcal{P}_{dk}} \sum_{l' \in \mathcal{P}_{dk}} \mathbb{E}\left\{ a_{kl'} a_{kl}^* \right\} + \sigma_d^2. \tag{42e}$$

As in the BBD case, the pilot-based DL channel estimation has negligible computational complexity, involving only a small number of complex multiplications per coherence interval that depend linearly on τ_{p_d}. These complex multiplications are necessary for projecting the received signal vector onto the pilot sequence and for calculating the covariances and variances of scalar random variables, which must then be multiplied by the projected received signal sample.

Theorem 2: For the distributed CB case, the APs (or the CPU) can compute the linear MMSE channel estimate $\hat{a}_{kk}^{\mathrm{pbd}}$ in closed form by using $\mathbb{E}\{a_{kk}\}$ as obtained in (32),

[3] Even though this algorithm is fully detailed in [3, Sec. 4.4], it is worth noting that it iteratively assigns pilots to the MSs by always selecting, in a greedy manner, the one that results in the least pilot contamination. This approach prevents worst-case scenarios where closely spaced MSs are assigned the same pilot. After the pilot sequences have been allocated, cluster formation is implemented by allowing each AP to serve exactly τ_{p_u} MSs. For each pilot, the AP serves the MS with the strongest channel gain among the subset of MSs assigned to that pilot.

$$\mathbb{E}\{\check{y}_{pk}\} = \sum_{l\in\mathcal{P}_k}\sum_{m\in\mathcal{M}_l}\sqrt{\frac{\tau_{p_d} p_{dml}}{\mathrm{tr}\left(\hat{\boldsymbol{R}}_{ml}\right)}}\mathrm{tr}\left(\hat{\boldsymbol{R}}_{mk}\boldsymbol{R}_{ml}\boldsymbol{R}_{mk}^{-1}\right), \quad (43)$$

with $\mathcal{P}_k = \mathcal{P}_{dk} \cap \mathcal{P}_{uk}$,

$$\begin{aligned}\mathbb{E}\{a_{kk}\check{y}_{pk}{}^*\} = &\sum_{l\in\mathcal{P}_k}\sum_{m\in\mathcal{M}_{kl}}\sqrt{\frac{\tau_{p_d} p_{dmk} p_{dml}}{\mathrm{tr}\left(\hat{\boldsymbol{R}}_{mk}\right)\mathrm{tr}\left(\hat{\boldsymbol{R}}_{ml}\right)}}\\ &\times\Bigg[\mathrm{tr}\left(\boldsymbol{R}_{mk}\hat{\boldsymbol{R}}_{mk}\boldsymbol{R}_{mk}^{-1}\boldsymbol{R}_{ml}\right)\\ &+\lambda_{mk}\Bigg[\mathrm{tr}\left(\boldsymbol{R}_{mk}\left(\hat{\boldsymbol{R}}_{mk}\boldsymbol{R}_{mk}^{-1}\right)^2\boldsymbol{R}_{ml}\right)\\ &+\mathrm{tr}\left(\hat{\boldsymbol{R}}_{mk}\right)\mathrm{tr}\left(\hat{\boldsymbol{R}}_{mk}\boldsymbol{R}_{mk}^{-1}\boldsymbol{R}_{ml}\right)\Bigg]\Bigg]\\ &+\sum_{l\in\mathcal{P}_k}\sum_{m'\in\mathcal{M}_k}\sum_{m\in\mathcal{M}_l}\sqrt{\frac{\tau_{p_d} p_{dm'k} p_{dml}}{\mathrm{tr}\left(\hat{\boldsymbol{R}}_{m'k}\right)\mathrm{tr}\left(\hat{\boldsymbol{R}}_{ml}\right)}}\\ &\times\mathrm{tr}\left(\hat{\boldsymbol{R}}_{m'k}\right)\mathrm{tr}\left(\hat{\boldsymbol{R}}_{mk}\boldsymbol{R}_{mk}^{-1}\boldsymbol{R}_{ml}\right), \quad (44)\end{aligned}$$

with $\mathcal{M}_{kl} = \mathcal{M}_k \cap \mathcal{M}_l$, and

$$\begin{aligned}\mathbb{E}\left\{\left|\check{y}_{pk}\right|^2\right\} = &\sum_{l\in\mathcal{P}_k}\sum_{l'\in\mathcal{P}_k}\sum_{m\in\mathcal{M}_{ll'}}\sqrt{\frac{\tau_{p_d}^2 p_{dml'} p_{dml}}{\mathrm{tr}\left(\hat{\boldsymbol{R}}_{ml'}\right)\mathrm{tr}\left(\hat{\boldsymbol{R}}_{ml}\right)}}\\ &\times\Bigg[\mathrm{tr}\left(\boldsymbol{R}_{mk}\boldsymbol{R}_{ml'}\boldsymbol{R}_{mk}^{-1}\hat{\boldsymbol{R}}_{mk}\boldsymbol{R}_{mk}^{-1}\boldsymbol{R}_{ml}\right)\\ &+\lambda_{mk}\Bigg[\mathrm{tr}\left(\boldsymbol{R}_{mk}\boldsymbol{R}_{ml'}\left(\boldsymbol{R}_{mk}^{-1}\hat{\boldsymbol{R}}_{mk}\right)^2\boldsymbol{R}_{mk}^{-1}\boldsymbol{R}_{ml}\right)\\ &+\mathrm{tr}\left(\hat{\boldsymbol{R}}_{mk}\boldsymbol{R}_{ml'}\boldsymbol{R}_{mk}^{-1}\right)\mathrm{tr}\left(\hat{\boldsymbol{R}}_{mk}\boldsymbol{R}_{mk}^{-1}\boldsymbol{R}_{ml}\right)\Bigg]\Bigg]\\ &+\sum_{l\in\mathcal{P}_k}\sum_{l'\in\mathcal{P}_k}\sum_{m'\in\mathcal{M}_{l'}}\sum_{m'\in\mathcal{M}_l}\sqrt{\frac{\tau_{p_d}^2 p_{dm'l'} p_{dml}}{\mathrm{tr}\left(\hat{\boldsymbol{R}}_{m'l'}\right)\mathrm{tr}\left(\hat{\boldsymbol{R}}_{ml}\right)}}\\ &\times\mathrm{tr}\left(\hat{\boldsymbol{R}}_{m'k}\boldsymbol{R}_{m'l'}\boldsymbol{R}_{m'k}^{-1}\right)\mathrm{tr}\left(\boldsymbol{R}_{mk}^{-1}\boldsymbol{R}_{ml}\hat{\boldsymbol{R}}_{mk}\right)\\ &+\sum_{\substack{l\in\mathcal{P}_{dk}\\ l\notin\mathcal{P}_{uk}}}\sum_{m\in\mathcal{M}_l}\frac{\tau_{p_d} p_{dml}}{\mathrm{tr}\left(\hat{\boldsymbol{R}}_{ml}\right)}\mathrm{tr}\left(\boldsymbol{R}_{mk}\hat{\boldsymbol{R}}_{ml}\right)+\sigma_d^2. \quad (45)\end{aligned}$$

Proof: See Appendix B. ∎

III. PERFORMANCE ANALYSIS

A. HARDENING RATIO

The channel hardening property of cell-free massive MIMO systems is essential when a generic MS k attempts to detect its desired signal solely based on the statistics of the effective channel gain a_{kk} (i.e., using the HBD strategy). With sufficient channel hardening, the effective channel gain a_{kk} converges to its mean value, allowing MS k to reliably utilize $\mathbb{E}\{a_{kk}\}$ as the true effective channel gain for detection. However, in scenarios with weak channel hardening, relying on $\mathbb{E}\{a_{kk}\}$ for signal detection can significantly compromise system performance. The robustness of channel hardening can be quantified using the channel hardening ratio, which is defined, for a specific MS k, as [23]

$$\mathrm{HR}_k = \frac{\mathrm{var}\{a_{kk}\}}{|\mathbb{E}\{a_{kk}\}|^2} = \frac{\mathbb{E}\{|a_{kk}|^2\}}{|\mathbb{E}\{a_{kk}\}|^2} - 1. \quad (46)$$

Note that a perfect channel hardening occurs whenever $\mathrm{var}\{a_{kk}\} = 0$ and, hence, $\mathrm{HR}_k = 0$.

Theorem 3: For the distributed CB case, the hardening ratio of the effective precoded channel between MS k and the set of APs in $\mathcal{M}_k$ can be computed in closed form by using $\mathbb{E}\{a_{kk}\}$ as obtained in (32), and

$$\begin{aligned}\mathrm{var}\{a_{kk}\} = &\sum_{m\in\mathcal{M}_k}\frac{p_{dmk}}{\mathrm{tr}\left(\hat{\boldsymbol{R}}_{mk}\right)}\Bigg[\mathrm{tr}\left(\hat{\boldsymbol{R}}_{mk}\boldsymbol{R}_{mk}\right)\\ &+\lambda_{mk}\left[\mathrm{tr}\left(\boldsymbol{R}_{mk}\hat{\boldsymbol{R}}_{mk}\boldsymbol{R}_{mk}^{-1}\hat{\boldsymbol{R}}_{mk}\right)+\left(\mathrm{tr}\left(\hat{\boldsymbol{R}}_{mk}\right)\right)^2\right]\Bigg] \quad (47)\end{aligned}$$

Proof: See Appendix B. ∎

The parameter λ_{mk}, defined in (34), is bounded by

$$\frac{1}{N_{mk}}\left(\sum_{j=1}^{N_{mk}}\left|c_{mkj}\right|^2\right)^2 \le \lambda_{mk} \le \sum_{j=1}^{N_{mk}}\left|c_{mkj}\right|^2, \quad (48)$$

where, as stated by Sutton et al. in [10], the lower bound follows from the application of the Cauchy-Schwarz inequality, and the upper bound is based on the fact that $|c_{mkj}|^2 \le 1$. Now, taking into account that $\sum_{j=1}^{N_{mk}}|c_{mkj}|^2 = 1$, it holds that

$$\frac{1}{N_{mk}} \le \lambda_{mk} \le 1. \quad (49)$$

The upper bound corresponds to the scenario in which the propagation channel between MS k and the mth AP is characterized by a single keyhole. The lower bound, in contrast, is attained when $|c_{mkj}|^2 = 1/N_{mk}$ for all $j \in \{1, \ldots, N_{mk}\}$. These results lead to the following insights with respect to the DL hardening ratio for the distributed CB case:

- First, the worst-case scenario arises when an MS receives signals from all its serving APs through single-keyhole channels. This specific condition leads to the weakest channel hardening situation (i.e., the largest hardening ratio).
- Second, for a given number of keyholes, the optimal scenario is a channel between a particular AP and a MS characterized by equal keyhole gains, as it leads to the strongest hardening ratio condition (i.e., the lowest hardening ratio).
- Third, as the number of keyholes through which an MS receives signals tends to infinity (i.e., as $N_{mk} \to \infty$), the propagation channel approximates a pure Ricean fading channel. In this case, the parameter λ_{mk} tends to zero, minimizing the hardening ratio and creating the best-case scenario for specific channel parameters, including the Ricean K-factor and the spatial correlation matrix of the NLOS component.

- Finally, using similar arguments as those employed in [7], it can be demonstrated that: (i) the presence of a dominant LOS component in the wireless link between a given MS and the corresponding APs enhances channel hardening, (ii) spatial correlation among the antennas at the APs results in weaker channel hardening metrics compared to a scenario with uncorrelated antennas, and (iii) the pure cell-free scheme, where all APs serve all MSs, represents the best-case scenario for channel hardening compared to any scalable UC strategy.

B. SPECTRAL EFFICIENCY

1) HBD STRATEGY

Assuming that MS k has only access to the average CSI $\mathbb{E}\{a_{kk}\}$, a deterministic number that can be easily obtained in practice without the need to transmit DL pilots, an achievable spectral efficiency of MS k can be obtained as [3, Th. 6.1]

$$\eta_k^{\text{hbd}} = \frac{\tau_d}{\tau_f}\log_2\left(1+\text{SINR}_k^{\text{hbd}}\right), \tag{50}$$

where the DL effective SINR can be expressed as

$$\text{SINR}_k^{\text{hbd}} = \frac{|\mathbb{E}\{a_{kk}\}|^2}{\sum_{l\in\mathcal{K}}\mathbb{E}\left\{|a_{kl}|^2\right\}-|\mathbb{E}\{a_{kk}\}|^2+\sigma_d^2}. \tag{51}$$

Theorem 4: For the distributed CB precoding case, the achievable spectral efficiency η_k^{hbd} can be expressed in closed form by using $\mathbb{E}\{a_{kk}\}$ as defined in (32) and

$$\begin{aligned}\sum_{l\in\mathcal{K}}\mathbb{E}\left\{|a_{kl}|^2\right\} &= \sum_{l\in\mathcal{K}}\sum_{m\in\mathcal{M}_l}\frac{p_{dml}}{\text{tr}\left(\hat{\boldsymbol{R}}_{ml}\right)}\text{tr}\left(\boldsymbol{R}_{mk}\hat{\boldsymbol{R}}_{ml}\right)\\ &+\sum_{l\in\mathcal{P}_{uk}}\left|\sum_{m\in\mathcal{M}_l}\sqrt{\frac{p_{dml}}{\text{tr}\left(\hat{\boldsymbol{R}}_{ml}\right)}}\text{tr}\left(\hat{\boldsymbol{R}}_{mk}\boldsymbol{R}_{ml}\boldsymbol{R}_{mk}^{-1}\right)\right|^2\\ &+\sum_{l\in\mathcal{P}_{uk}}\sum_{m\in\mathcal{M}_l}\frac{p_{dml}}{\text{tr}\left(\hat{\boldsymbol{R}}_{ml}\right)}\lambda_{mk}\\ &\times\left[\text{tr}\left(\boldsymbol{R}_{mk}\boldsymbol{R}_{ml}\left(\boldsymbol{R}_{mk}^{-1}\hat{\boldsymbol{R}}_{mk}\right)^2\boldsymbol{R}_{mk}^{-1}\boldsymbol{R}_{ml}\right)\right.\\ &\left.+\text{tr}\left(\hat{\boldsymbol{R}}_{mk}\boldsymbol{R}_{ml}\boldsymbol{R}_{mk}^{-1}\right)\text{tr}\left(\hat{\boldsymbol{R}}_{mk}\boldsymbol{R}_{mk}^{-1}\boldsymbol{R}_{ml}\right)\right]\Big],\end{aligned} \tag{52}$$

in (51).

Proof: See Appendix B. ∎

By employing arguments akin to those articulated in the section focused on the assessment of channel hardening and leveraging Theorem 4, significant insights concerning the spectral efficiency dynamics when employing a distributed CB precoder and the HBD strategy can be gleaned:

- First, the self-interference term resulting from the channel estimation error experienced by a particular MS k contains components that are multiplied by λ_{mk}. As this parameter is maximized when the MS receives signals through single-keyhole channels, this condition leads to the worst-case situation in terms of achievable spectral efficiency. In other words, the spectral efficiency that an HBD-based CF-mMIMO network might offer to an MS experiencing single-keyhole channel propagation can be seriously compromised.
- Second, the parameter λ_{mk} decreases as the number of effective keyholes characterizing the propagation channel MS k and AP m increases. Moreover, for a given number of keyholes, λ_{mk} is minimized when all of them have exactly the same gain. Consequently, the achievable spectral efficiency experienced by a particular MS increases with the number of surrounding keyholes, specially when they have similar gains.
- For an infinite number of keyholes, the propagation channels behave as pure Ricean fading channels. In this case, the parameter λ_{mk} equals zero, causing the corresponding components in the self-interference term to vanish. As a result, the achievable spectral efficiency increases.

2) BBD AND PBD STRATEGIES

The received DL signal at MS k, expressed in (13), can be rewritten as

$$y_{dk}(t) = a_{kk}s_k(t)+\tilde{n}_{dk}(t), \tag{53}$$

where

$$\tilde{n}_{dk}(t) = \sum_{\substack{l\in\mathcal{K}\\ l\neq k}}a_{kl}s_l(t)+n_{dk}(t). \tag{54}$$

Note that, when implementing the PBD strategy, $s_k(t)$ is independent of a_{kk}^{pbd} and of $\hat{a}_{kk}$, $\tilde{n}_{dk}(t)$ has zero mean, and $s_k(t)$ and $\tilde{n}_{dk}(t)$, when conditioned on $\hat{a}_{kk}$, are uncorrelated since

$$\begin{aligned}\mathbb{E}\left\{\tilde{n}_{dk}(t)|\hat{a}_{kk}^{\text{pbd}}\right\} &= \mathbb{E}\left\{s_k^*(t)\tilde{n}_{dk}(t)|\hat{a}_{kk}^{\text{pbd}}\right\}\\ &= \mathbb{E}\left\{a_{kk}^*s_k^*(t)\tilde{n}_{dk}(t)|\hat{a}_{kk}^{\text{pbd}}\right\}=0.\end{aligned} \tag{55}$$

Hence, the achievable spectral efficiency can be obtained using [18, eq. (2.46)] as

$$\eta_k^{\text{pbd}} = \frac{\tau_d}{\tau_f}\mathbb{E}\left\{\log_2\left(1+\text{SINR}_k^{\text{pbd}}\right)\right\}, \tag{56}$$

with

$$\text{SINR}_k^{\text{pbd}} = \frac{\left|\mathbb{E}\left\{a_{kk}|\hat{a}_{kk}^{\text{pbd}}\right\}\right|^2}{\sum_{l\in\mathcal{K}}\mathbb{E}\left\{|a_{kl}|^2|\hat{a}_{kk}^{\text{pbd}}\right\}-\left|\mathbb{E}\left\{a_{kk}|\hat{a}_{kk}^{\text{pbd}}\right\}\right|^2+\sigma_d^2}, \tag{57}$$

where the outer expectation in (56) is obtained with respect to $\hat{a}_{kk}^{\text{pbd}}$.

As already mentioned in Section II-D, the constraints in (55) do not hold for the BBD case when using the channel estimate obtained in (29). Just for the purpose of calculating an achievable spectral efficiency, the aforementioned issue can be addressed by approximating $\hat{a}_{kk}^{\text{bbd}}$ with $\hat{a}_{kk}^{\text{bbd}}(t)$ and substituting $\hat{a}_{kk}^{\text{pbd}}$ with $\hat{a}_{kk}^{\text{bbd}}(t)$ in (55)-(57) (see [13, Sec. V]

for more details) to obtain ${\eta_k}^{\text{bbd}}$ and ${\text{SINR}_k}^{\text{bbd}}$. Note that in this case, for the sake of conciseness and with a slight abuse of notation, we will continue using analytical expressions written in terms of $\hat{a}_{kk}^{\text{bbd}}$ instead of explicitly employing $\hat{a}_{kk}^{\text{bbd}}(t)$.

Since the random variables $\{a_{kl}\}$ are not Gaussian distributed, their estimates $\{\hat{a}_{kl}^{\text{xbd}}\}$, where xbd is a token used to denote either the BBD (i.e., xbd = bbd) or the PBD (i.e., xbd = pbd) strategies, and corresponding estimation errors are uncorrelated, but not independent. This makes computing the expectations in ${\text{SINR}_k}^{\text{bbd}}$ and ${\text{SINR}_k}^{\text{pbd}}$ challenging, if at all possible, in closed form. As suggested by Ngo and Larsson in [13], however, these expectations can be numerically computed by first using Bayes' theorem and then the Riemann integration rule in such a way that

$$ {\eta_k}^{\text{xbd}} = \frac{\tau_d}{\tau_f} \sum_i \Delta_{x_i} p_{\hat{a}_{kk}^{\text{xbd}}}(x_i) \log_2\Big(1 + {\text{SINR}_k}^{\text{xbd}}(x_i)\Big), \quad (58) $$

with

$$ {\text{SINR}_k}^{\text{xbd}}(x_i) = \frac{|\mathbb{E}\{a_{kk}|x_i\}|^2}{\sum_{l\in\mathcal{K}} \mathbb{E}\{|a_{kl}|^2|x_i\} - |\mathbb{E}\{a_{kk}|x_i\}|^2 + \sigma_d^2}, \quad (59) $$

and

$$ \mathbb{E}\{a_{kk}|x_i\} \approx \sum_j y_j \Delta_{y_j} \frac{p_{a_{kk},\hat{a}_{kk}^{\text{xbd}}}(y_j, x_i)}{p_{\hat{a}_{kk}^{\text{xbd}}}(x_i)}, \quad (60a) $$

$$ \mathbb{E}\Big\{|a_{kl}|^2|x_i\Big\} \approx \sum_n z_n \Delta_{z_n} \frac{p_{|a_{kl}|^2,\hat{a}_{kk}^{\text{xbd}}}(z_n, x_i)}{p_{\hat{a}_{kk}^{\text{xbd}}}(x_i)}, \quad (60b) $$

where Δ_{x_i}, Δ_{y_j} and Δ_{z_n} denote the sizes of the ith, jth and nth intervals of the partitions used in the corresponding Riemann integration processes. Moreover, the probability density function $p_{\hat{a}_{kk}^{\text{xbd}}}(x_i)$, as well as the joint density functions $p_{a_{kk},\hat{a}_{kk}^{\text{xbd}}}(y_j, x_i)$ and $p_{|a_{kl}|^2,\hat{a}_{kk}^{\text{xbd}}}(y_j, x_i)$ can be obtained using standard numerical computing tools.

3) PERFECT DL CSI

For benchmarking purposes, let us also consider the idealistic scenario where perfect CSI is available at the MSs. In this ideal case, the useful term in (13) is $a_{kk}s_k(t)$ and, consequently, the achievable spectral efficiency of MS k can be expressed as [3]

$$ {\eta_k}^{\text{ideal}} = \frac{\tau_d}{\tau_f} \mathbb{E}\left\{ \log_2\left(1 + \frac{|a_{kk}|^2}{\sum_{\substack{l\in\mathcal{K} \\ l\neq k}} |a_{kl}|^2 + \sigma_d^2}\right)\right\}. \quad (61) $$

IV. NUMERICAL RESULTS

Following the common practice in the literature on CF-mMIMO networking (see, for instance, [3] and references therein), APs and MSs are uniformly distributed within a square coverage area with a side length of D meters. Additionally, to emulate the effects of a large network deployment without edges, a wrap-around topology is used where all APs and MSs experience equivalent interference conditions.

TABLE 3. Summary of default simulation parameters.

Parameter	Value
Side of the square coverage area: D	1000 m
Number of APs: M	80 APs
Number of antennas at the APs: N	2 antennas
Number of MSs: K	20 MSs
Noise variance: $\sigma_u^2 = \sigma_d^2$	-94 dBm
Available average power at the AP: P_d	200 mW
Available average power at the MS: P_p	100 mW
Power control coefficients: υ, κ, ϖ	-0.5, 0.5, 0.5
Frame length: τ_f	200 samples
Training phase length: $\tau_{p_u} = \tau_{p_d}$	15 samples
LOS reference distance: d_0	20 m
Pathloss parameters: α, β, σ_χ	
- Case LOS, $10m < d_{mk} \leq 150m$	34, 2.2, 3
- Case LOS, $d_{mk} > 150m$	-5.17, 4, 3
- Case NLOS	30, 3.67, 4
Shadow fading decorrelation distance: d_{dcorr}	9 m
Shadow fading correlation among APs:	0.5
Ricean K-factor distribution: μ_K, σ_K	9 dB, 5 dB
Keyhole probability: p_{KH}	0.3
Number of keyholes: N_{KH}	2 keyholes
Angular standard deviations (ASDs)	15°

The probability of a MS being in a keyhole scenario is set to a fixed value denoted as p_{KH}, and the number of keyholes characterizing the propagation channels of MSs in such a situation are set to a constant value $N_{mk} = N_{\text{KH}}$, with $|c_{mkj}|^2 = 1/N_{\text{KH}}$. The links between the mth AP and the N_{mk} keyholes, which characterize the environment surrounding the kth MS, are classified as either LOS or NLOS, with the LOS probability determined by [24]

$$ p_{\text{LOS}}(d_{mk}) = \min\left(1, \frac{d_0}{d_{mk}} + \left(1 - \frac{d_0}{d_{mk}}\right) e^{-\frac{d_{mk}}{2d_0}}\right), \quad (62) $$

where d_0 and d_{mk} denote a reference distance and the distance between AP m and MS k, respectively. The Ricean K-factor is set to $K_{mk} = 0$ for NLOS propagation links. For LOS propagation links it is characterized as $10\log_{10}(K_{mk}) \sim \mathcal{N}(\mu_k, {\sigma_k}^2)$. The propagation gain of the link between the mth AP and the kth MS can be expressed as

$$ \beta_{mk} = 10^{(\alpha + 10\beta\log_{10}(d_{mk}) + \chi_{mk})/10}, \quad (63) $$

with $\chi_{mk} \sim \mathcal{N}(0, \sigma_\chi^2)$ denoting the shadow fading component, whose spatial correlation model is described in [4, (54)-(55)]. The parameters α, β and σ_χ vary depending on whether the link is in LOS or NLOS conditions.

Each AP is assumed to be equipped with a N-antenna uniform linear array (ULA) located on the xy-plane and with half wavelength antenna spacing. The generic analytical expression for the antenna array response vector at the

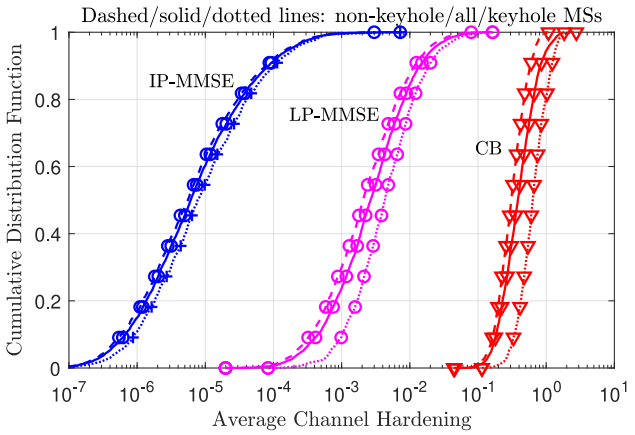

FIGURE 2. CDFs of the DL hardening ratio achieved when using CB, LP-MMSE or IP-MMSE precoding ($M = 80$ APs, $K = 20$ MSs, $N = 2$ antennas per AP).

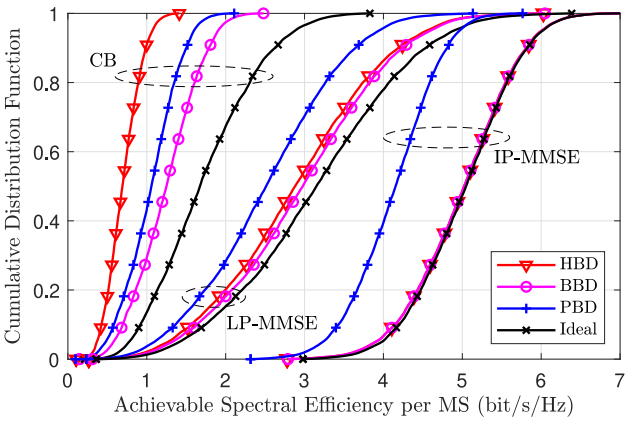

FIGURE 3. CDFs of the achievable spectral efficiency per MS for the different channel estimation and precoding strategies evaluated in this work ($M = 80$ APs, $K = 20$ MSs, $N = 2$ antennas per AP).

azimuth and elevation angles φ and ϑ can then be expressed as

$$\boldsymbol{a}(\varphi, \vartheta) = \left[1 \; e^{j\pi \sin\varphi \cos\vartheta} \; \ldots \; e^{j\pi(N-1)\sin\varphi\cos\vartheta}\right]. \quad (64)$$

Moreover, considering the Gaussian local scattering model described in [3, Sec. 2.6], where the scattering components are distributed around the nominal azimuth and elevation angles according to a Gaussian distribution, the components of the spatial correlation matrix $\boldsymbol{C}_{mk}$ can be computed using [3, eqs. (2.18)-(2.19)].

Default parameters used to set-up the simulation scenarios under evaluation are summarized in Table 2 and are inspired by prior research works on this topic (see, for instance, [3], [4], [24], [25] and references therein). Remarkably, it has been assumed that in the HBD, BBD and Ideal cases, $\tau_{p_u} = 15$ samples, $\tau_u = \lceil(\tau_f - \tau_{p_u})/2\rceil$ and $\tau_d = \tau_f - \tau_{p_u} - \tau_u$. In the PBD case, in contrast, it has been assumed that $\tau_{p_u} = \tau_{p_d} = 15$ samples, $\tau_u = \lceil(\tau_f - \tau_{p_u})/2\rceil$ and $\tau_d = \tau_f - \tau_{p_u} - \tau_{p_d} - \tau_u$. Moreover, the DCC scheme described in [3, Sec. 4.4] is used to allocate the available training sequences to MSs.

Figure 2 shows the CDF of the channel hardening coefficient averaged across the MSs in the network (solid lines), using the CB, LP-MMSE, and IP-MMSE precoders, and assuming the default system parameters provided in Table 3. Furthermore, it also presents the CDFs of the average channel hardening coefficient for MSs either not subject to propagation through keyhole channels (dashed lines) or subject to propagation through keyhole channels (dotted lines). A key observation from these graphs is that the centralized IP-MMSE precoder offers significantly better channel hardening coefficients (much closer to zero) compared to distributed precoding schemes. Additionally, among the distributed schemes, the LP-MMSE precoder performs notably better than the CB precoder. These performance differences can be quite large, with the median channel hardening coefficient being $6.1 \cdot 10^{-6}$ for IP-MMSE, $2.6 \cdot 10^{-3}$ for LP-MMSE, and $3.8 \cdot 10^{-1}$ for CB. These results suggest that DL channel estimation at the MSs may be completely unnecessary in systems using centralized precoding and could yield substantial improvements in systems using distributed precoding schemes, particularly with CB precoding. As expected, MSs subject to propagation through keyholes experience significantly worse channel hardening coefficients compared to those that do not.

In Fig. 3, well-known results within the realm of CF-mMIMO systems are clearly visible. Firstly, centralized precoding offers significantly better achievable spectral efficiency metrics than distributed precoding. Secondly, among the distributed precoders, the CB scheme provides achievable spectral efficiencies that are considerably lower than those provided by the LP-MMSE precoder. However, these are not the most interesting findings that can be drawn from the analysis of the graphs presented in this figure. The most interesting results lie in the fact that different precoding schemes exhibit very different channel hardening coefficients, as seen in Fig. 2, and consequently, their impact on the behavior of the various detection schemes that are analyzed in this paper will also be quite different. Firstly, it can be observed that since the system based on IP-MMSE exhibits very good channel hardening coefficients (very close to zero), the HBD scheme, which is based on the assumption that massive MIMO-based systems exhibit channel hardening, delivers performance metrics very close to that of the ideal system. The BBD scheme provides slightly better performance (almost imperceptible in the figure) than the HBD scheme. However, this slight performance gain does not seem to justify the increased complexity associated with the blind channel estimation process. The PBD-based scheme, although it provides an accurate channel estimation, does so at the cost of reducing the number of coherence block samples dedicated to data transmission. Therefore, the performance improvement due to better channel estimation does not compensate for the performance losses due to the decrease in the value of the ratio τ_d/τ_f.

The proposed detection schemes behave radically differently when the CB precoding scheme is used. In this case, since the channel hardening coefficients are high (i.e.,

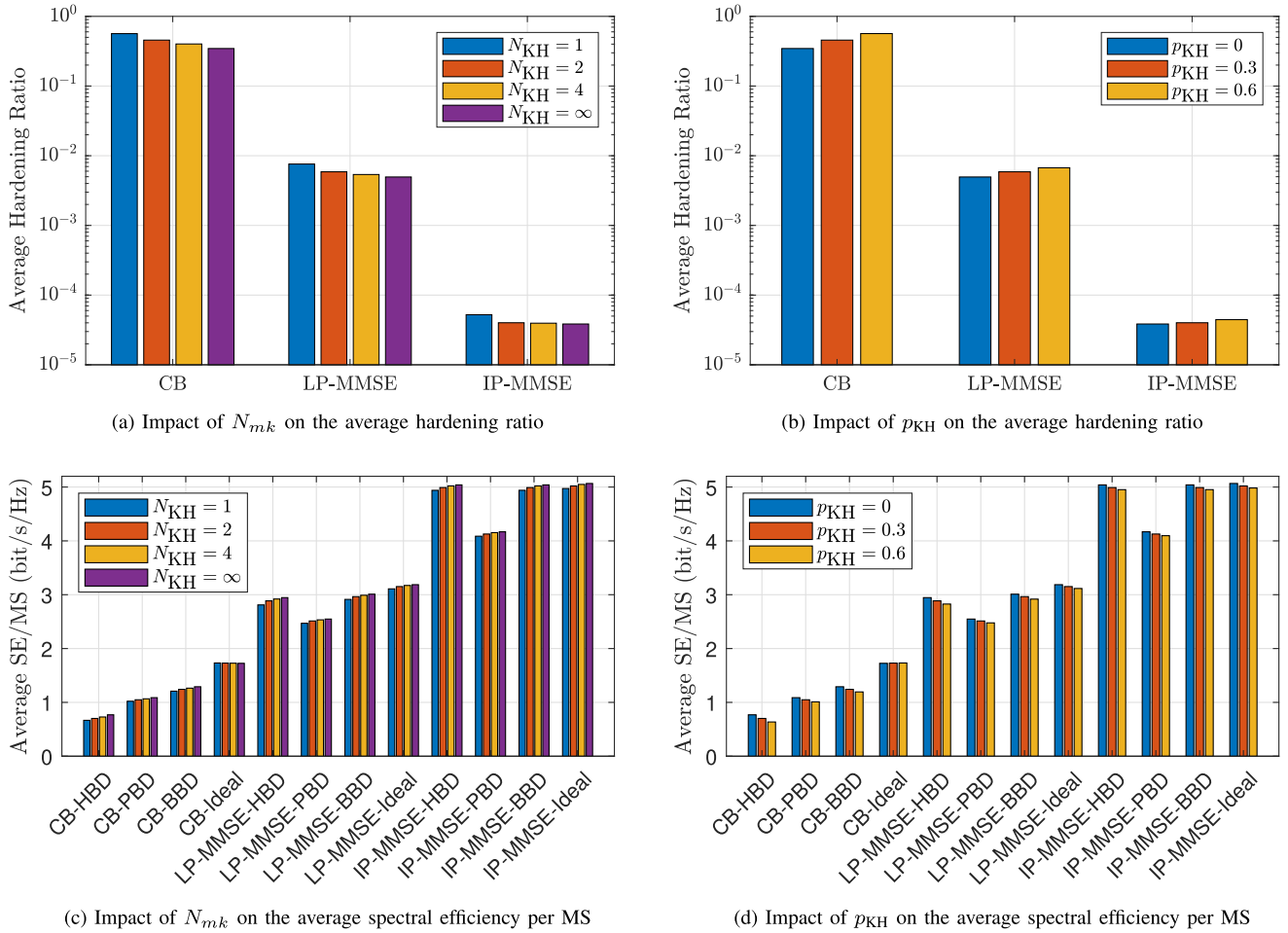

(a) Impact of N_{mk} on the average hardening ratio

(b) Impact of p_{KH} on the average hardening ratio

(c) Impact of N_{mk} on the average spectral efficiency per MS

(d) Impact of p_{KH} on the average spectral efficiency per MS

FIGURE 4. Impact of N_{mk} and p_{KH} on the average hardening ratio and spectral efficiency per MS for the different channel estimation and precoding strategies evaluated in this work.

channel hardening is very weak), the HBD scheme provides achievable spectral efficiencies that are far from what an ideal scheme (i.e., a genie-based scheme) would offer. This fact makes the implementation of detection schemes based on effective channel estimation, both the BBD and PBD schemes, worthwhile. It is interesting to note, however, that the PBD scheme provides lower performance than the BBD scheme. In other words, the blind estimation, although it provides a lower quality channel estimation, compensates for this because it does not use samples from the coherence interval to transmit pilot sequences.

Focusing now on the performance of the different detection schemes when using an LP-MMSE precoder, we observe, as expected, that its behavior falls between that of the CB and IP-MMSE schemes. Specifically, the performance of the HBD scheme tends to that of the ideal scheme but still leaves a considerable margin for improvement. This margin for improvement, as in the case of the CB precoder, is considerably exploited by the BBD scheme. The PBD scheme, as in the case of the IP-MMSE precoder, is unable to compensate for the losses due to the decrease in the ratio τ_d/τ_f.

The general conclusions that can be drawn from the results presented in Figs. 2 and 3 are: i) the centralized IP-MMSE precoder provides almost perfect channel hardening and, therefore, the use of the HBD scheme offers nearly ideal performance, making the use of detection schemes based on the estimation of the effective channel unnecessary, ii) the distributed precoding schemes, especially CB, do not provide sufficient channel hardening and, therefore, the use of detection schemes based on the estimation of the effective channel might be justified, and iii) the PBD scheme provides worse performance metrics than the BBD scheme and, in scenarios using MMSE precoders, whether distributed or centralized, it performs even worse than the HBD scheme. However, these results were obtained assuming a scenario characterized by default system parameters provided in Table 3. Next, results will be presented aiming at evaluating the impact the variations in some of these parameters might have on the aforementioned conclusions.

Figure 4 presents results that allow for evaluating the impact the variation of some of the parameters characterizing the multiple keyhole spatially correlated Ricean fading channel might have on the average hardening ratio and the average

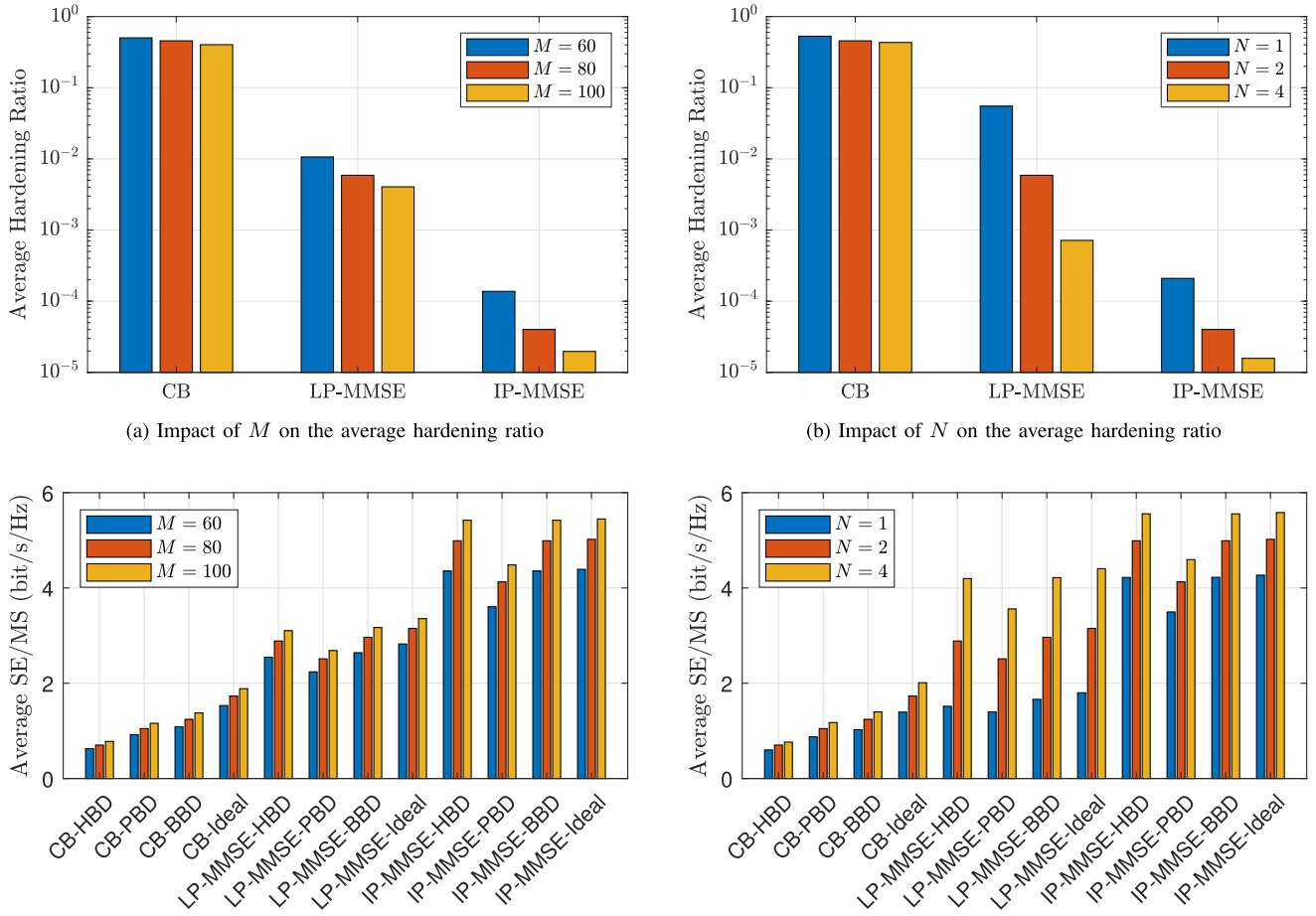

(a) Impact of M on the average hardening ratio

(b) Impact of N on the average hardening ratio

(c) Impact of M on the average spectral efficiency per MS

(d) Impact of N on the average spectral efficiency per MS

FIGURE 5. **Impact of *M* and *N* on the average hardening ratio and spectral efficiency per MS for the different channel estimation and precoding strategies evaluated in this work.**

achievable spectral efficiency per MS. Specifically, Figs. 4(a) and 4(c) show that an increase in the number of keyholes translates into an improvement in both metrics, and that this improvement is relatively more significant when using the CB precoder compared to the LP-MMSE and especially the IP-MMSE precoders. A very similar effect can be observed in Figures 4(b) and 4(d) as the probability that an MS is subject to propagation channels through keyholes decreases.[4] However, the most important takeaway from these results is that, even under the worst propagation conditions (i.e., channels with a single keyhole or scenarios with a very high probability of propagation through keyholes), the BBD scheme offers no significant advantage over HBD when using centralized precoding, and the use of PBD is counterproductive. Another interesting conclusion is that even under the best propagation conditions (i.e., propagation through pure Ricean fading channels), CB precoding and even LP-MMSE do not guarantee channel hardening levels high enough to make the use of the BBD scheme unjustifiable.

[4]Note that the numerical results obtained for $N_{\mathrm{KH}} = \infty$ coincide with those obtained when $p_{\mathrm{KH}} = 0$.

In Fig. 5, the impact of variations in network infrastructure (i.e., the number of APs and/or the number of antennas per AP) on the average hardening ratio and the average achievable spectral efficiency per MS is evaluated. It is well known that, in a massive MIMO system, increasing the number of antennas serving the MSs translates to an increase in channel hardening. This fact is clearly demonstrated in the results presented in Figs. 5(a) and 5(b), where $M \in \{60, 80, 100\}$ and $N \in \{1, 2, 4\}$, respectively. However, these results reveal an even more interesting fact: the LP-MMSE and IP-MMSE precoders are capable of better leveraging the increase in the number of APs and, especially, the increase in the number of antennas per AP. Actually, the improvement in the hardening ratio is significantly greater when these precoders are used, which also results in markedly different behaviors of the various proposed detection schemes. The case that stands out the most is the behavior of the LP-MMSE precoder as the number of antennas per AP is varied. For single-antenna APs, the level of channel hardening is quite moderate, and both the PBD and BBD schemes provide better spectral efficiencies than the HBD scheme. However, for APs equipped with $N = 4$ antennas, there is

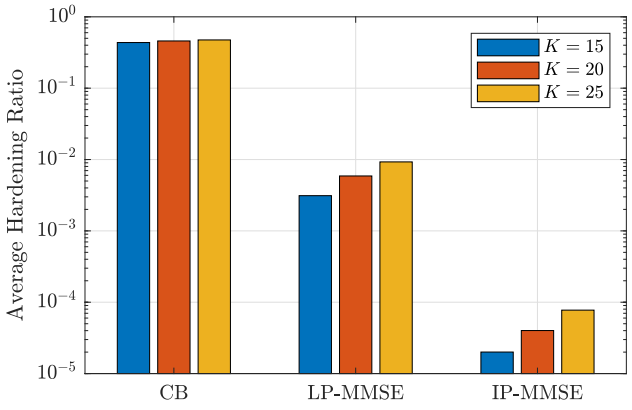

(a) Impact of K on the average hardening ratio

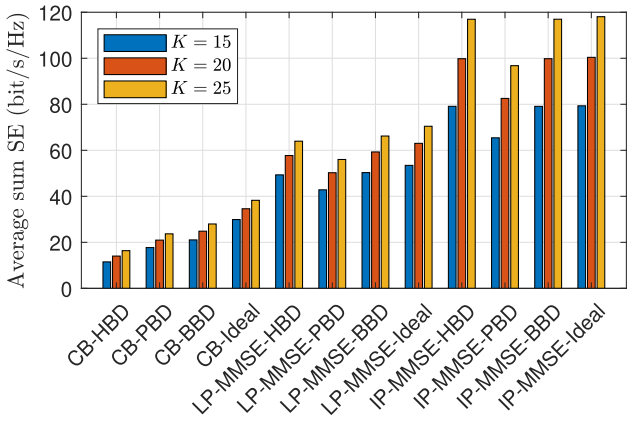

(b) Impact of K on the average sum spectral efficiency

FIGURE 6. Impact of K on the average hardening ratio and sum spectral efficiency for the different channel estimation and precoding strategies evaluated in this work.

a considerable improvement in channel hardening, and the performance metrics of the HBD scheme far surpass those of the PBD scheme, and approach those of the BBD scheme up to the point where implementing this detection scheme would become rather unjustifiable. Moreover, the performance of this precoder comes so close to that of the centralized IP-MMSE that it could eventually make it difficult to justify the increased complexity typically associated with such precoders.

In a CF-mMIMO network, varying the number of MSs while keeping the total number of antennas in the network fixed should produce similar effects to those observed when varying the number of antennas in the network while keeping the number of MSs fixed, as shown in the results presented in Fig. 5. This can be easily verified by evaluating the results in Fig. 6, where different network loads with $K = 15$, 20, or 25 MSs have been evaluated in a CF-mMIMO network with $M = 80$ APs, each equipped with $N = 2$ antennas. As the number of MSs increases, the average number of APs serving each of the MSs decreases, resulting in weaker hardening ratio metrics. However, increasing the network load is associated with a higher level of multiuser diversity. Thus, even though the spectral efficiency per MS decreases,

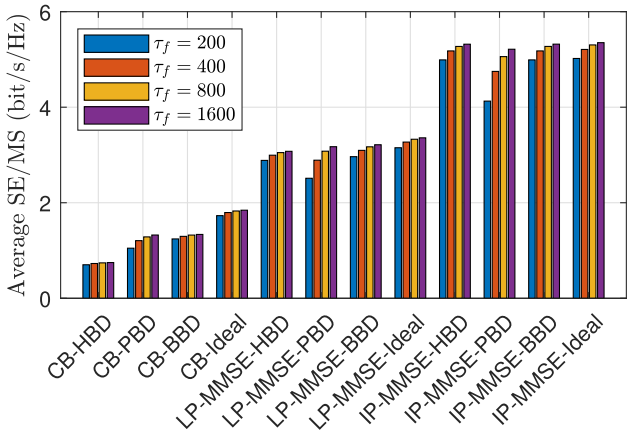

FIGURE 7. Impact of τ_f on the average spectral efficiency per MS for the different channel estimation and precoding strategies evaluated in this work.

the global spectral efficiency of the network (i.e., the sum of spectral efficiencies achieved by all MSs in the network), as shown in Fig. 6(b), increases. The most noteworthy result from Fig. 6, however, is that the LP-MMSE and IP-MMSE precoders are more affected by the variation of K, similar to what happened with the variations of M and N.

Despite the quality of channel estimations based on pilot transmission in the DL, in all the scenarios analyzed in the previous figures, the performance of the PBD scheme has consistently been inferior to that of the BBD scheme and, in most cases, especially when using MMSE-based precoders, even inferior to that provided by the HBD scheme. Thus, it seems pertinent to ask whether there is indeed any scenario where pilot-based channel estimation could be justified over the blind-based channel estimation. Given that the fundamental issue with the PBD scheme lies in the fact that the availability of pilot-based channel estimates does not compensate for the reduction of the quotient τ_d/τ_f, Fig. 7 presents results obtained as the value of τ_f is increased while keeping the value of τ_{pd} fixed, hence ensuring $\tau_d/\tau_f \to 1/2$. Obviously, this would only be possible in scenarios with a very large coherence interval (i.e., scenarios with very low levels of temporal and/or frequency selectivity). What we can observe in this figure is that, indeed, as the value of τ_f increases, the spectral efficiency of the schemes based on PBD approaches that of the schemes based on BBD. However, even in the case where $\tau_f = 1600$ samples, it does not surpass it. Therefore, an important conclusion to be drawn from these results is that, in CF-mMIMO systems with single-antenna MSs, blind channel estimation is considerably more advisable than pilot-based channel estimation.

V. CONCLUSION

In the context of beyond-5G and 6G wireless networks, CF-mMIMO has established itself as a pivotal architecture, effectively meeting the escalating needs for seamless connectivity and high data throughput. In this research work an in-depth investigation has been conducted into scalable UC CF-mMIMO systems, emphasizing the importance of DL CSI acquisition (either instantaneous or statistical) and

its complex interplay with the implementation of both distributed and centralized precoding techniques. The analysis presented in this paper particularly focuses on the critical role of DL CSI acquisition in scenarios characterized by weak channel hardening, which can result from sparse subsets of APs serving specific MSs under UC strategies, and the transmission over spatially correlated multiple keyhole Ricean fading channels.

Answering the set of questions that were posed in Section I-B, our research has revealed that even though the number of APs serving an MS can be relatively small when implementing a scalable UC CF-mMIMO network, the MSs experience sufficient channel hardening when relying on statistical CSI if powerful centralized precoders are implemented at the APs, even when transmitting in single-keyhole spatially correlated fading scenarios. The channel hardening metrics are much weaker when using distributed precoding schemes, especially when relying on CB. Specifically, the centralized IP-MMSE precoding scheme demonstrates near-perfect channel hardening, effectively eliminating the need for detection schemes based on instantaneous effective channel estimation in favor of those based on statistical CSI. In the realm of distributed precoding strategies, the LP-MMSE scheme clearly outperforms the conventional CB precoding, showcasing its superior capability in these contexts. However, distributed precoding schemes, particularly the CB strategy, fail to provide adequate channel hardening, thereby justifying the use of detection schemes based on instantaneous effective channel estimation.

Blind channel estimation schemes, which have already demonstrated their ability to improve the DL performance of cellular massive MIMO systems, can also provide significant performance improvements in UC CF-mMIMO network deployments, properly adapting to multi-keyhole spatially correlated fading channels and outperforming the DL training-based schemes. In fact, our findings indicate that, among the instantaneous DL effective channel estimation strategies, pilot-based decoding schemes consistently underperform relative to blind-based decoding approaches. This is primarily because the improved channel estimation quality they offer does not compensate for the spectral efficiency losses associated with the DL pilot transmission overhead. Hence, in UC CF-mMIMO systems using distributed precoding to convey payload data to single-antenna MSs, the implementation of DL decoding schemes based on blind channel estimation is considerably more advisable than those relying on pilot-based channel estimation.

Increasing the number of APs in the network or the number of antennas per AP always helps improve the performance metrics of the system. Using APs equipped with a large number of antennas, however, is especially beneficial when implementing interference-aware precoding schemes such as the distributed LP-MMSE or the centralized IP-MMSE.

The aforementioned insights underscore the critical importance of selecting appropriate precoding and decoding strategies to optimize channel hardening and overall network efficiency in UC CF-mMIMO systems, especially when transmitting in scenarios with weak channel hardening conditions.

APPENDIX A
USEFUL RESULTS

Lemma 1: Given a complex Gaussian random vector $\boldsymbol{x} \sim \mathcal{CN}_N(\boldsymbol{0}, \boldsymbol{I}_N)$ and two arbitrary matrices $\boldsymbol{A} \in \mathbb{C}^{N\times N}$ and $\boldsymbol{B} \in \mathbb{C}^{N\times N}$, the first moments of the complex quadratic form $\mathcal{Q} = \boldsymbol{x}^H\boldsymbol{A}\boldsymbol{x}$ and the complex quartic form $\mathcal{Q}_2 = \boldsymbol{x}^H\boldsymbol{A}\boldsymbol{x}\boldsymbol{x}^H\boldsymbol{B}\boldsymbol{x}$ can be obtained as

$$\mathbb{E}\{\mathcal{Q}\} = \mathrm{tr}(\boldsymbol{A}) \tag{A.1}$$

and

$$\mathbb{E}\{\mathcal{Q}_2\} = \mathrm{tr}(\boldsymbol{A}\boldsymbol{B}) + \mathrm{tr}(\boldsymbol{A})\ \mathrm{tr}(\boldsymbol{B}). \tag{A.2}$$

Proof: Let us define x_i as the ith component of vector $\boldsymbol{v}$ and a_{ij} and b_{ij} as the (i,j)th components of the matrices $\boldsymbol{A}$ and $\boldsymbol{B}$, respectively. Using these definitions, the complex quadratic form can be expressed as

$$\mathcal{Q} = \sum_{i=1}^{N}\sum_{j=1}^{N} a_{ij}x_i^*x_j. \tag{A.3}$$

Hence, the first moment of $\mathcal{Q}$ can be expressed as

$$\mathbb{E}\{\mathcal{Q}\} = \sum_{i=1}^{N}\sum_{j=1}^{N} a_{ij}\mathbb{E}\{x_i^*x_j\} = \sum_{i=1}^{N} a_{ii} = \mathrm{tr}(\boldsymbol{A}). \tag{A.4}$$

Analogously, the first moment of $\mathcal{Q}_2$ can be expressed as

$$\mathbb{E}\{\mathcal{Q}_2\} = \sum_{i=1}^{N}\sum_{j=1}^{N}\sum_{q=1}^{N}\sum_{l=1}^{N} a_{ij}b_{ql}\mathbb{E}\{x_i^*x_jx_qx_l^*\}. \tag{A.5}$$

Taking into account that

$$\mathbb{E}\{x_i^*x_jx_q^*x_l\} = \begin{cases} 2,\ i=j=q=l \\ 1,\ j=i,\ \ l=q,\ \ q\neq i \\ 1,\ l=i,\ \ q=j,\ \ j\neq i \\ 0,\ \text{otherwise,} \end{cases} \tag{A.6}$$

we obtain

$$\begin{aligned}\mathbb{E}\{\mathcal{Q}_2\} &= 2\sum_{i=1}^{N} a_{ii}b_{ii} + \sum_{i=1}^{N}\sum_{\substack{q=1\\q\neq i}}^{N} a_{ii}b_{qq} + \sum_{i=1}^{N}\sum_{\substack{j=1\\j\neq i}}^{N} a_{ij}b_{ji} \\ &= \sum_{i=1}^{N} a_{ii}\sum_{q=1}^{N} b_{qq} + \sum_{i=1}^{N}\sum_{j=1}^{N} a_{ij}b_{ji} \\ &= \mathrm{tr}(\boldsymbol{A})\ \mathrm{tr}(\boldsymbol{B}) + \mathrm{tr}(\boldsymbol{A}\boldsymbol{B}). \end{aligned} \tag{A.7}$$

■

Lemma 2: Given a multiple keyhole spatially correlated Ricean fading channel $\boldsymbol{h}_{mk}$, as described in (1), and two arbitrary matrices $\boldsymbol{A} \in \mathbb{C}^{N\times N}$ and $\boldsymbol{B} \in \mathbb{C}^{N\times N}$, then

$$\mathbb{E}\left\{\boldsymbol{h}_{mk}^H \boldsymbol{A}\boldsymbol{h}_{mk}\right\} = \mathrm{tr}(\boldsymbol{R}_{mk}\boldsymbol{A}), \tag{A.8}$$

and

$$\mathbb{E}\left\{\boldsymbol{h}_{mk}^H \boldsymbol{A}\boldsymbol{h}_{mk}\boldsymbol{h}_{mk}^H \boldsymbol{B}\boldsymbol{h}_{mk}\right\} = (\lambda_{mk}+1) \times[\mathrm{tr}(\boldsymbol{R}_{mk}\boldsymbol{A})\mathrm{tr}(\boldsymbol{R}_{mk}\boldsymbol{B}) + \mathrm{tr}(\boldsymbol{R}_{mk}\boldsymbol{A}\boldsymbol{R}_{mk}\boldsymbol{B})]. \tag{A.9}$$

Proof: Using $\boldsymbol{g}_{mkj} = \boldsymbol{R}_{mk}^{1/2}\bar{\boldsymbol{g}}_{mkj}$ in (1), with $\bar{\boldsymbol{g}}_{mkj} \sim \mathcal{CN}_N(\boldsymbol{0}, \boldsymbol{I}_N)$, and relying on the fact that α_{mki} and α_{mkj}, as well as $\bar{\boldsymbol{g}}_{mki}$ and $\bar{\boldsymbol{g}}_{mkj}$, are uncorrelated for all $i \neq j$, it holds that

$$\mathbb{E}\left\{\boldsymbol{h}_{mk}^H \boldsymbol{A}\boldsymbol{h}_{mk}\right\} = \sum_{i=1}^{N_{mk}} |c_{mki}|^2 \mathbb{E}\left\{\bar{\boldsymbol{g}}_{mki}^H \boldsymbol{R}_{mk}^{H/2}\boldsymbol{A}\boldsymbol{R}_{mk}^{1/2}\bar{\boldsymbol{g}}_{mki}^H\right\}. \tag{A.10}$$

Now, using $\sum_{i=1}^{N_{mk}} |c_{mki}|^2 = 1$ and applying (A.1), result (A.8) follows.

Analogously, the expectation in (A.9) can be expressed as

$$\begin{aligned}\mathbb{E}&\left\{\boldsymbol{h}_{mk}^H \boldsymbol{A}\boldsymbol{h}_{mk}\boldsymbol{h}_{mk}^H \boldsymbol{B}\boldsymbol{h}_{mk}\right\} \\ &= \sum_{i=1}^{N_{mk}}\sum_{j=1}^{N_{mk}}\sum_{q=1}^{N_{mk}}\sum_{l=1}^{N_{mk}} c_{mki}^* c_{mkj} c_{mkq}^* c_{mkl} \\ &\quad\times\mathbb{E}\left\{\alpha_{mki}^*\alpha_{mkj}\alpha_{mkq}^*\alpha_{mkl}\right\} \\ &\quad\times\mathbb{E}\left\{\bar{\boldsymbol{g}}_{mki}^H\overline{\boldsymbol{A}}\bar{\boldsymbol{g}}_{mkj}\bar{\boldsymbol{g}}_{mkq}^H\overline{\boldsymbol{B}}\bar{\boldsymbol{g}}_{mkl}\right\}.\end{aligned} \tag{A.11}$$

with $\overline{\boldsymbol{A}} = \boldsymbol{R}_{mk}^{H/2}\boldsymbol{A}\boldsymbol{R}_{mk}^{1/2}$ and $\overline{\boldsymbol{B}} = \boldsymbol{R}_{mk}^{H/2}\boldsymbol{B}\boldsymbol{R}_{mk}^{1/2}$. As the random variables α_{mki}, for $i \in \{1, \ldots, N_{mk}\}$, are iid as $\alpha_{mki} \sim \mathcal{CN}(0,1)$, the result presented in (A.6) also holds when substituting x_i with α_{mki}. Hence,

$$\begin{aligned}\mathbb{E}&\left\{\boldsymbol{h}_{mk}^H \boldsymbol{A}\boldsymbol{h}_{mk}\boldsymbol{h}_{mk}^H \boldsymbol{B}\boldsymbol{h}_{mk}\right\} \\ &= 2\sum_{i=1}^{N_{mk}} |c_{mki}|^4 \mathbb{E}\left\{\bar{\boldsymbol{g}}_{mki}^H\overline{\boldsymbol{A}}\bar{\boldsymbol{g}}_{mki}\bar{\boldsymbol{g}}_{mki}^H\overline{\boldsymbol{B}}\bar{\boldsymbol{g}}_{mki}\right\} \\ &\quad+\sum_{i=1}^{N_{mk}} |c_{mki}|^2 \sum_{\substack{q=1\\q\neq i}}^{N_{mk}} |c_{mkq}|^2 \mathbb{E}\left\{\bar{\boldsymbol{g}}_{mki}^H\overline{\boldsymbol{A}}\bar{\boldsymbol{g}}_{mki}\right\} \\ &\quad\times\mathbb{E}\left\{\bar{\boldsymbol{g}}_{mkq}^H\overline{\boldsymbol{B}}\bar{\boldsymbol{g}}_{mkq}\right\} \\ &\quad+\sum_{i=1}^{N_{mk}} |c_{mki}|^2 \sum_{\substack{j=1\\j\neq i}}^{N_{mk}} |c_{mkj}|^2 \mathbb{E}\left\{\bar{\boldsymbol{g}}_{mki}^H\overline{\boldsymbol{A}}\,\overline{\boldsymbol{B}}\bar{\boldsymbol{g}}_{mki}\right\}.\end{aligned} \tag{A.12}$$

Now, using (A.1) and (A.2), grouping terms and taking into account that $\sum_{i=1}^{N_{mk}} |c_{mki}|^2 = 1$ and $\sum_{i=1}^{N_{mk}} |c_{mki}|^4 = \lambda_{mk}$, it is easy to demonstrate that result (A.9) holds. ■

Lemma 3: Given a multiple keyhole spatially correlated Ricean fading channel $\boldsymbol{h}_{mk}$, as described in (1), the corresponding linear MMSE channel estimate $\hat{\boldsymbol{h}}_{mk}$, as described in (7), and two arbitrary matrices $\boldsymbol{A} \in \mathbb{C}^{N\times N}$ and $\boldsymbol{B} \in \mathbb{C}^{N\times N}$, then

$$\mathbb{E}\left\{\boldsymbol{h}_{mk}^H \boldsymbol{A}\hat{\boldsymbol{h}}_{mk}\right\} = \mathbb{E}\left\{\hat{\boldsymbol{h}}_{mk}^H \boldsymbol{A}\hat{\boldsymbol{h}}_{mk}\right\} = \mathrm{tr}\left(\hat{\boldsymbol{R}}_{mk}\boldsymbol{A}\right), \tag{A.13}$$

and

$$\begin{aligned}\mathbb{E}&\left\{\boldsymbol{h}_{mk}^H \boldsymbol{A}\hat{\boldsymbol{h}}_{mk}\hat{\boldsymbol{h}}_{mk}^H \boldsymbol{B}\boldsymbol{h}_{mk}\right\} \\ &= (\lambda_{mk}+1)\mathrm{tr}\left(\hat{\boldsymbol{R}}_{mk}\boldsymbol{A}\right)\mathrm{tr}\left(\hat{\boldsymbol{R}}_{mk}\boldsymbol{B}\right) \\ &\quad+\lambda_{mk}\mathrm{tr}\left(\boldsymbol{R}_{mk}\boldsymbol{A}\hat{\boldsymbol{R}}_{mk}\boldsymbol{R}_{mk}^{-1}\hat{\boldsymbol{R}}_{mk}\boldsymbol{B}\right) \\ &\quad+\mathrm{tr}\left(\boldsymbol{R}_{mk}\boldsymbol{A}\hat{\boldsymbol{R}}_{mk}\boldsymbol{B}\right).\end{aligned} \tag{A.14}$$

Proof: Using the definitions of $\boldsymbol{y}_{mk}$ and $\hat{\boldsymbol{h}}_{mk}$ presented in (6) and (7), respectively, and applying result (A.8) yields

$$\begin{aligned}\mathbb{E}\left\{\boldsymbol{h}_{mk}^H \boldsymbol{A}\hat{\boldsymbol{h}}_{mk}\right\} &= \sqrt{\tau_{p_u}P_{p_u}}\,\mathbb{E}\left\{\boldsymbol{h}_{mk}^H \boldsymbol{A}\boldsymbol{R}_{mk}\boldsymbol{\Psi}_{mk}^{-1}\boldsymbol{y}_{mk}\right\} \\ &= \tau_{p_u}P_{p_u}\mathbb{E}\left\{\boldsymbol{h}_{mk}^H \boldsymbol{A}\boldsymbol{R}_{mk}\boldsymbol{\Psi}_{mk}^{-1}\boldsymbol{h}_{mk}\right\} \\ &= \tau_{p_u}P_{p_u}\mathrm{tr}\left(\boldsymbol{A}\boldsymbol{R}_{mk}\boldsymbol{\Psi}_{mk}^{-1}\boldsymbol{R}_{mk}\right).\end{aligned} \tag{A.15}$$

Now, using the definition of $\hat{\boldsymbol{R}}_{mk}$ in (9), result (A.13) follows.

Let us define $\boldsymbol{A}_{mk} = \boldsymbol{A}\boldsymbol{R}_{mk}\boldsymbol{\Psi}_{mk}^{-1}$ and $\boldsymbol{B}_{mk} = \boldsymbol{\Psi}_{mk}^{-1}\boldsymbol{R}_{mk}\boldsymbol{B}$. Using these definitions and those of $\boldsymbol{y}_{mk}$ and $\hat{\boldsymbol{h}}_{mk}$ we have that

$$\begin{aligned}\mathbb{E}&\left\{\boldsymbol{h}_{mk}^H \boldsymbol{A}\hat{\boldsymbol{h}}_{mk}\hat{\boldsymbol{h}}_{mk}^H \boldsymbol{B}\boldsymbol{h}_{mk}\right\} \\ &= \tau_{p_u}P_{p_u}\mathbb{E}\left\{\boldsymbol{h}_{mk}^H \boldsymbol{A}_{mk}\boldsymbol{y}_{mk}\boldsymbol{y}_{mk}^H \boldsymbol{B}_{mk}\boldsymbol{h}_{mk}\right\} \\ &= \left(\tau_{p_u}P_{p_u}\right)^2\mathbb{E}\left\{\boldsymbol{h}_{mk}^H \boldsymbol{A}_{mk}\boldsymbol{h}_{mk}\boldsymbol{h}_{mk}^H \boldsymbol{B}_{mk}\boldsymbol{h}_{mk}\right\} \\ &\quad+\left(\tau_{p_u}P_{p_u}\right)^2\sum_{\substack{l\in\mathcal{P}_{uk}\\l\neq k}}\mathbb{E}\left\{\boldsymbol{h}_{mk}^H \boldsymbol{A}_{mk}\boldsymbol{R}_{ml}\boldsymbol{B}_{mk}\boldsymbol{h}_{mk}\right\} \\ &\quad+\tau_{p_u}P_{p_u}\sigma_u^2\mathbb{E}\left\{\boldsymbol{h}_{mk}^H \boldsymbol{A}_{mk}\boldsymbol{B}_{mk}\boldsymbol{h}_{mk}\right\}.\end{aligned} \tag{A.16}$$

The expectations on the right hand side (RHS) of this equation can be solved in closed form by applying results (A.8) and (A.9) yielding

$$\begin{aligned}\mathbb{E}&\left\{\boldsymbol{h}_{mk}^H \boldsymbol{A}\hat{\boldsymbol{h}}_{mk}\hat{\boldsymbol{h}}_{mk}^H \boldsymbol{B}\boldsymbol{h}_{mk}\right\} \\ &= \left(\tau_{p_u}P_{p_u}\right)^2(\lambda_{mk}+1)\left[\mathrm{tr}(\boldsymbol{R}_{mk}\boldsymbol{A}_{mk}\boldsymbol{R}_{mk}\boldsymbol{B}_{mk})\right. \\ &\quad\left.+\mathrm{tr}(\boldsymbol{R}_{mk}\boldsymbol{A}_{mk})\mathrm{tr}(\boldsymbol{R}_{mk}\boldsymbol{B}_{mk})\right] \\ &\quad+\left(\tau_{p_u}P_{p_u}\right)^2\sum_{\substack{l\in\mathcal{P}_{uk}\\l\neq k}}\mathrm{tr}(\boldsymbol{R}_{mk}\boldsymbol{A}_{mk}\boldsymbol{R}_{ml}\boldsymbol{B}_{mk}) \\ &\quad+\tau_{p_u}P_{p_u}\sigma_u^2\mathrm{tr}(\boldsymbol{R}_{mk}\boldsymbol{A}_{mk}\boldsymbol{B}_{mk}\}.\end{aligned} \tag{A.17}$$

Finally, grouping terms and taking into account the definitions of $\boldsymbol{\Psi}_{mk}$ and $\hat{\boldsymbol{R}}_{mk}$, the result (A.14) straightforwardly follows. ■

APPENDIX B
PROOF OF THEOREMS IN SECTION II

For the distributed CB case, we have that

$$\begin{aligned}\mathbb{E}\{a_{kl}\} &= \mathbb{E}\left\{\boldsymbol{h}_{\mathcal{M}_l k}^H \boldsymbol{w}_l\right\} = \sum_{m\in\mathcal{M}_l}\mathbb{E}\left\{\boldsymbol{h}_{mk}^H \boldsymbol{w}_{ml}\right\} \\ &= \sum_{m\in\mathcal{M}_l}\sqrt{\frac{p_{d_{ml}}}{\mathrm{tr}\left(\hat{\boldsymbol{R}}_{ml}\right)}}\,\mathbb{E}\left\{\boldsymbol{h}_{mk}^H \hat{\boldsymbol{h}}_{ml}\right\}\end{aligned}$$

$$= \begin{cases} \sum_{m\in\mathcal{M}_l} \sqrt{\frac{p_{dml}}{\mathrm{tr}\left(\hat{\boldsymbol{R}}_{ml}\right)}}\mathbb{E}\left\{\boldsymbol{h}_{mk}^H \boldsymbol{R}_{ml}\boldsymbol{R}_{mk}^{-1}\hat{\boldsymbol{h}}_{mk}\right\}, & l \in \mathcal{P}_{uk} \\ 0, & l \notin \mathcal{P}_{uk} \end{cases}$$
$$= \begin{cases} \sum_{m\in\mathcal{M}_l} \sqrt{\frac{p_{dml}}{\mathrm{tr}\left(\hat{\boldsymbol{R}}_{ml}\right)}}\mathrm{tr}\left(\hat{\boldsymbol{R}}_{mk}\boldsymbol{R}_{ml}\boldsymbol{R}_{mk}^{-1}\right), & l \in \mathcal{P}_{uk} \\ 0, & l \notin \mathcal{P}_{uk}, \end{cases} \tag{B.1}$$

where in the last equality we have used (A.1). Note that this result directly leads to (43). Moreover, upon setting $l = k$, result (32) follows, which is also used in Theorems 2 to 4.

Let us now proceed to analyze the term $\mathbb{E}\{a_{kl'}a_{kl}^*\}$ for the case in which a distributed CB precoder is used, as follows

$$\mathbb{E}\{a_{kl'}a_{kl}^*\} = \mathbb{E}\left\{\boldsymbol{h}_{\mathcal{M}_{l'}k}^H \boldsymbol{w}_{l'}\boldsymbol{w}_l^H \boldsymbol{h}_{\mathcal{M}_l k}\right\}$$
$$= \sum_{m'\in\mathcal{M}_{l'}}\sum_{m\in\mathcal{M}_l} \sqrt{\frac{p_{dm'l'}p_{dml}}{\mathrm{tr}\left(\hat{\boldsymbol{R}}_{m'l'}\right)\mathrm{tr}\left(\hat{\boldsymbol{R}}_{ml}\right)}}$$
$$\times\mathbb{E}\left\{\boldsymbol{h}_{m'k}^H\hat{\boldsymbol{h}}_{m'l'}\hat{\boldsymbol{h}}_{ml}^H\boldsymbol{h}_{mk}\right\}. \tag{B.2}$$

The calculation of $\mathbb{E}\{\boldsymbol{h}_{m'k}^H\hat{\boldsymbol{h}}_{m'l'}\hat{\boldsymbol{h}}_{ml}^H\boldsymbol{h}_{mk}\}$ can be split in two different cases:

1) *Case $m' \neq m$*: In this case, the channel responses and channel estimates corresponding to AP m are uncorrelated with those corresponding to AP m' and hence,

$$\mathbb{E}\left\{\boldsymbol{h}_{m'k}^H\hat{\boldsymbol{h}}_{m'l'}\hat{\boldsymbol{h}}_{ml}^H\boldsymbol{h}_{mk}\right\} = \mathbb{E}\left\{\boldsymbol{h}_{m'k}^H\hat{\boldsymbol{h}}_{m'l'}\right\}\mathbb{E}\left\{\hat{\boldsymbol{h}}_{ml}^H\boldsymbol{h}_{mk}\right\}$$
$$= \begin{cases} \mathbb{E}\left\{\boldsymbol{h}_{m'k}^H\boldsymbol{R}_{m'l'}\boldsymbol{R}_{m'k}^{-1}\hat{\boldsymbol{h}}_{m'k}\right\} \\ \quad\times\mathbb{E}\left\{\hat{\boldsymbol{h}}_{mk}^H\boldsymbol{R}_{mk}^{-1}\boldsymbol{R}_{ml}\boldsymbol{h}_{mk}\right\}, & l,\ l' \in \mathcal{P}_{uk} \\ 0, & \text{otherwise} \end{cases}$$
$$= \begin{cases} \mathrm{tr}\left(\hat{\boldsymbol{R}}_{m'k}\boldsymbol{R}_{m'l'}\boldsymbol{R}_{m'k}^{-1}\right) \\ \quad\times\mathrm{tr}\left(\boldsymbol{R}_{mk}^{-1}\boldsymbol{R}_{ml}\hat{\boldsymbol{R}}_{mk}\right), & l,\ l' \in \mathcal{P}_{uk} \\ 0, & \text{otherwise}, \end{cases} \tag{B.3}$$

where, in the last equality, result (A.13) has been applied.

2) *Case $m' = m$*: In this case we have that

$$\mathbb{E}\left\{\boldsymbol{h}_{mk}^H\hat{\boldsymbol{h}}_{ml'}\hat{\boldsymbol{h}}_{ml}^H\boldsymbol{h}_{mk}\right\}$$
$$= \begin{cases} \mathbb{E}\left\{\boldsymbol{h}_{mk}^H\boldsymbol{R}_{ml'}\boldsymbol{R}_{mk}^{-1}\hat{\boldsymbol{h}}_{mk}\hat{\boldsymbol{h}}_{mk}^H\boldsymbol{R}_{mk}^{-1}\boldsymbol{R}_{ml}\boldsymbol{h}_{mk}\right\}, & l,\ l' \in \mathcal{P}_{uk} \\ \mathbb{E}\left\{\boldsymbol{h}_{mk}^H\mathbb{E}\left\{\hat{\boldsymbol{h}}_{ml}\hat{\boldsymbol{h}}_{ml}^H\right\}\boldsymbol{h}_{mk}\right\}, & l' = l \notin \mathcal{P}_{uk} \\ 0, & \text{otherwise} \end{cases}$$
$$= \begin{cases} (\lambda_{mk}+1)\mathrm{tr}\left(\hat{\boldsymbol{R}}_{mk}\boldsymbol{R}_{ml'}\boldsymbol{R}_{mk}^{-1}\right)\mathrm{tr}\left(\hat{\boldsymbol{R}}_{mk}\boldsymbol{R}_{mk}^{-1}\boldsymbol{R}_{ml}\right) \\ \quad+\lambda_{mk}\mathrm{tr}\left(\boldsymbol{R}_{mk}\boldsymbol{R}_{ml'}\left(\boldsymbol{R}_{mk}^{-1}\hat{\boldsymbol{R}}_{mk}\right)^2\boldsymbol{R}_{mk}^{-1}\boldsymbol{R}_{ml}\right) \\ \quad+\mathrm{tr}\left(\boldsymbol{R}_{mk}\boldsymbol{R}_{ml'}\boldsymbol{R}_{mk}^{-1}\hat{\boldsymbol{R}}_{mk}\boldsymbol{R}_{mk}^{-1}\boldsymbol{R}_{ml}\right), & l,\ l' \in \mathcal{P}_{uk} \\ \mathrm{tr}\left(\boldsymbol{R}_{mk}\hat{\boldsymbol{R}}_{ml}\right), & l' = l \notin \mathcal{P}_{uk} \\ 0, & \text{otherwise}, \end{cases} \tag{B.4}$$

where, in the last equality, results (A.14) and (A.8) have been applied.

Substituting the results obtained in the previous two cases into (B.2), expressions (33), (44), (45), (47), and (52) can be straightforwardly derived.

REFERENCES

[1] H. He, X. Yu, J. Zhang, S. Song, and K. B. Letaief, "Cell-free massive MIMO for 6G wireless communication networks," *J. Commun. Inf. Netw.*, vol. 6, no. 4, pp. 321–335, 2021.

[2] H. Q. Ngo, G. Interdonato, E. G. Larsson, G. Caire, and J. G. Andrews, "Ultra-dense cell-free massive MIMO for 6G: Technical overview and open questions," 2024, *arXiv:2401.03898*.

[3] O. T. Demir, E. Björnson, and L. Sanguinetti, "Foundations of user-centric cell-free massive MIMO," *Found. Trends® Signal Process.*, vol. 14, nos. 3–4, pp. 162–472, 2021.

[4] H. Q. Ngo, A. Ashikhmin, H. Yang, E. G. Larsson, and T. L. Marzetta, "Cell-free massive MIMO versus small cells," *IEEE Trans. Wireless Commun.*, vol. 16, no. 3, pp. 1834–1850, Mar. 2017.

[5] Z. Chen and E. Björnson, "Channel hardening and Favorable propagation in cell-free massive MIMO with stochastic geometry," *IEEE Trans. Commun.*, vol. 66, no. 11, pp. 5205–5219, Nov. 2018.

[6] S. Willhammer, J. Flordelis, L. Van Der Perre, and F. Tufvesson, "Channel hardening in massive MIMO: Model parameters and experimental assessment," *IEEE Open J. Commun. Soc.*, vol. 1, pp. 501–512, 2020.

[7] A. A. Polegre, F. Riera-Palou, G. Femenias, and A. G. Armada, "Channel hardening in cell-free and user-centric massive MIMO networks with spatially correlated Ricean fading," *IEEE Access*, vol. 8, pp. 139827–139845, 2020.

[8] G. Interdonato, H. Q. Ngo, P. Frenger, and E. G. Larsson, "Downlink training in cell-free massive MIMO: A blessing in disguise," *IEEE Trans. Wireless Commun.*, vol. 18, no. 11, pp. 5153–5169, Nov. 2019.

[9] G. Femenias, F. Riera-Palou, A. Álvarez-Polegre, and A. García-Armada, "Short-term power constrained cell-free massive-MIMO over spatially correlated Ricean fading," *IEEE Trans. Veh. Technol.*, vol. 69, no. 12, pp. 15200–15215, Dec. 2020.

[10] J. A. C. Sutton, H. Q. Ngo, and M. Matthaiou, "Hardening the channels by precoder design in massive MIMO with multiple-antenna users," *IEEE Trans. Veh. Technol.*, vol. 70, no. 5, pp. 4541–4556, May 2021.

[11] G. Levin and S. Loyka, "On the outage capacity distribution of correlated keyhole MIMO channels," *IEEE Trans. Inf. Theory*, vol. 54, no. 7, pp. 3232–3245, Jul. 2008.

[12] C. Zhong, S. Jin, K.-K. Wong, and M. R. McKay, "Ergodic mutual information analysis for multi-keyhole MIMO channels," *IEEE Trans. Wireless Commun.*, vol. 10, no. 6, pp. 1754–1763, Jun. 2011.

[13] H. Q. Ngo and E. G. Larsson, "No downlink pilots are needed in TDD massive MIMO," *IEEE Trans. Wireless Commun.*, vol. 16, no. 5, pp. 2921–2935, May 2017.

[14] P. Pasangi, M. Atashbar, and M. Mohassel Feghhi, "Blind downlink channel estimation of multi-user multi-cell massive MIMO system in presence of the pilot contamination," *AEU Int. J. Electron. Commun.*, vol. 117, Apr. 2020, Art. no. 153099.

[15] A. Ghazanfari, T. Van Chien, E. Björnson, and E. G. Larsson, "Model-based and data-driven approaches for downlink massive MIMO channel estimation," *IEEE Trans. Commun.*, vol. 70, no. 3, pp. 2085–2101, Mar. 2022.

[16] D. D. Souza, M. M. M. Freitas, G. S. Borges, A. M. Cavalcante, D. B. da Costa, and J. C. W. A. Costa, "Effective channel blind estimation in cell-free massive MIMO networks," *IEEE Wireless Commun. Lett.*, vol. 11, no. 3, pp. 468–472, Mar. 2022.

[17] G. Femenias, F. Riera-Palou, and E. Björnson, "Another twist to the scalability in cell-free massive MIMO networks," *IEEE Trans. Commun.*, vol. 71, no. 11, pp. 6793–6804, Nov. 2023.

[18] T. Marzetta, E. Larsson, H. Yang, and H. Ngo, *Fundamentals of Massive MIMO*. Cambridge, U.K.: Cambridge Univ., 2016.

[19] R. Nikbakht, R. Mosayebi, and A. Lozano, "Uplink fractional power control and downlink power allocation for cell-free networks," *IEEE Wireless Commun. Lett.*, vol. 9, no. 6, pp. 774–777, Jun. 2020.

[20] S. Chen, J. Zhang, E. Björnson, J. Zhang, and B. Ai, "Structured massive access for scalable cell-free massive MIMO systems," *IEEE J. Sel. Areas Commun.*, vol. 39, no. 4, pp. 1086–1100, Apr. 2021.

[21] E. Björnson and L. Sanguinetti, "Scalable cell-free massive MIMO systems," *IEEE Trans. Commun.*, vol. 68, no. 7, pp. 4247–4261, Jul. 2020.
[22] G. Interdonato, E. Björnson, H. Quoc Ngo, P. Frenger, and E. G. Larsson, "Ubiquitous cell-free massive MIMO communications," *EURASIP J. Wireless Commun. Netw.*, vol. 2019, no. 1, pp. 1–13, 2019.
[23] Z. Chen, F. Sohrabi, and W. Yu, "Sparse activity detection for massive connectivity," *IEEE Trans. Signal Process.*, vol. 66, no. 7, pp. 1890–1904, Apr. 2018.
[24] "Study on 3D channel model for LTE; (Release 12), Version 12.7.0," 3GPP, Sophia Antipolis, France, Rep. 36.873, Dec. 2017.
[25] E. Björnson and L. Sanguinetti, "Making cell-free massive MIMO competitive with MMSE processing and centralized implementation," *IEEE Trans. Wireless Commun.*, vol. 19, no. 1, pp. 77–90, Jan. 2020.

GUILLEM FEMENIAS (Senior Member, IEEE) received the Telecommunication Engineer degree and the Ph.D. degree in electrical engineering from the Technical University of Catalonia (UPC), Barcelona, Spain, in 1987 and 1991, respectively.

From 1987 to 1994, he worked as a Researcher with UPC, where he became an Associate Professor in 1992. In 1995, he joined the Department of Mathematics and Informatics, University of the Balearic Islands (UIB), Spain, where he became Full Professor in 2010. He is currently leading the Mobile Communications Group, UIB, where he has been the Project Manager of numerous projects funded by the Spanish and Balearic Islands Governments. In the past, he was also involved with several European projects. His current research interests and activities span the fields of digital communications theory and wireless communication systems, with particular emphasis on radio resource management strategies applied to 5G and 6G wireless networks. On these topics, he has published more than 100 journal and conference papers, as well as some book chapters.

Dr. Femenias was the recipient of the Best Paper Awards at the 2007 IFIP International Conference on Personal Wireless Communications and at the 2009 IEEE Vehicular Technology Conference - Spring. He has served for various IEEE conferences as a technical program committee member, as the Publication Chair for the IEEE 69th Vehicular Technology Conference (Spring) in 2009, and as a Local Organizing Committee Member of the IEEE Statistical Signal Processing in 2016.

FELIP RIERA-PALOU (Senior Member, IEEE) received the B.S./M.S. degree in computer engineering from the University of the Balearic Islands (UIB), Mallorca, Spain, in 1997, the M.Sc. and Ph.D. degrees in communication engineering from the University of Bradford, U.K., in 1998 and 2002, respectively, and the M.Sc. degree in statistics from the University of Sheffield, U.K., in 2006.

From May 2002 to March 2005, he was with Philips Research Laboratories, Eindhoven, The Netherlands, first as a Marie Curie Postdoctoral Fellow (European Union) and later as a technical staff member. While at Philips, he worked on research programs related to wideband speech/audio compression and speech enhancement for mobile telephony. From April 2005 to December 2009, he was a Research Associate (Ramon y Cajal Program, Spanish Ministry of Science) with the Mobile Communications Group, Department of Mathematics and Informatics, UIB, where he has been an Associate Research Professor (I3 Program, Spanish Ministry of Education) since January 2010. His current research interests are in the general areas of signal processing and wireless communications.